Functional Analysis of Collapsin Response Mediator Protein 4 in Recovery after Neural Injury

神経損傷後の回復における Collapsin Response Mediator Protein 4 の機能解明

July 2015

Jun NAGAI

長井 淳

Functional Analysis of Collapsin Response Mediator Protein 4 in Recovery after Neural Injury

神経損傷後の回復における Collapsin Response Mediator Protein 4 の機能解明

July 2015

Waseda University
Graduate School of Advanced Science and Engineering
Department of Life Science and Medical Bioscience,
Research on Molecular Brain Science

Jun NAGAI

長井 淳

Contents

Abstract

There is currently no promising treatment for spinal cord injury (SCI) because severed spinal axons are not restored in the mammalian adult central nervous system (CNS). Axonal outgrowth inhibitors and scar formation are two major obstacles to CNS repair. Although a number of inhibitors were suggested to greatly contribute to the failure of CNS regeneration, sufficient regeneration after CNS injury was not provided with neither suppression of axonal inhibitors nor scar degradation with enzymes and anti-inflammatory molecules. Therefore, identification of a target molecule that regulates both axonal growth and scarring has been desired. Cytoskeletal dynamics is a key factor limiting regenerative capacity in the CNS in terms of axonal extension, inflammation and scarring. Collapsin response mediator protein 4 (CRMP4), a common downstream molecule of several inhibitory signaling pathways, is known to directly regulate cytoskeletal dynamics, but its roles in recovery after CNS injury *in vivo* remain elucidated.

Here, I focused on the role of CRMP4 in axonal responses *in vitro* against myelin-associated glycoprotein (MAG), one of the axon growth inhibitors, and the role

of CRMP4 in injured spinal cords *in vivo*. My *in vitro* study showed that MAG-induced inhibition of axonal outgrowth and axonal protection required CRMP4. Next, I identified CRMP4 as a crucial factor that contributes to both axonal growth inhibition and scarring after SCI. I found increases in the inhibitory and toxic forms of CRMP4 in injured spinal cord. Notably, CRMP4 expression was evident in activated microglia/macrophages and reactive astrocytes as well as in neurons after spinal cord transection. *Crmp4*−/− mice displayed neuroprotective effects against SCI and reductions in inflammatory response and scar formation. This permissive environment for axonal growth due to CRMP4 suppression restored locomotor activity at an unusually early phase of healing. These results suggest that suppression of CRMP4 is a unique therapeutic strategy that overcomes the two obstacles to CNS repair after SCI.

Chapter 1. Introduction

Injured adult mammalian CNS has limited regenerative ability. Recovery after CNS injury is potently restricted by two main obstacles: axon growth inhibitors and scar formation[1–3]. I describe in this chapter the scientific background of discovery of these obstacles and the reasons why I focused on CRMP4.

1.1 Central and peripheral nervous system

"In adult central nervous system the nerve paths are something fixed, ended, immutable. Everything may die, nothing may be regenerated." This statement from the father of modern neuroscience Santiago Ramón y Cajal means that different responses to injury are observed in the central nervous system (CNS) and in the peripheral nervous system (PNS) of the adult mammals[4]. While lesioned PNS axons successfully elongate and form synaptic connections with separated targets[5,6], the regenerative capacity of injured axons in the CNS is abortively limited, which leads to permanent loss of functions[7]. The possibility of an inherent disability of CNS regeneration has been nullified, because CNS axons grow over long distances into grafted peripheral nerve explants in the brain

or spinal cord[8]. Nonetheless, cultured peripheral axons are restricted to enter adult CNS tissues[9], suggesting that neurite growth inhibitors exists specifically in the adult CNS.

1.2 Myelin-associated inhibitors (MAIs)

The most different factor in the environment of CNS from that of PNS is the cell type ensheathing axons; oligodendrocyte in the CNS and Schwan cell in the PNS. Schwann cells produce various kinds of neurotropic factors, extracellular matrix, and adhesion molecules required for the growth-supporting properties of PNS axons[5,10]. In contrast, proteins inhibiting neurite outgrowth are shown to present within the membrane of oligodendrocytes, CNS myelin *in vitro*[11]. The significance of these myelin-associated inhibitors (MAIs) was implicated by a study showing that neurons growing *in vitro* with high concentrations of neurotrophic factors were incompetent to extend neurites into CNS explants[9]. Schwab and his colleagues successfully neutralized these inhibitory activities using monoclonal antibodies (IN-I, IN-2) against MAIs to allow neurite growth in culture on CNS myelin[12]. These antibodies were applied to rats with spinal cord lesion, which resulted in long-distance regrowth of corticospinal tract (CST) axons[13]. However, these experiments were not conclusive on the underlying

mechanisms.

Currently three MAIs are found[14]. The first isolated molecule of MAIs is one of the components of myelin called myelin-associated glycoprotein (MAG). MAG was shown to have a potent inhibitory activity to CNS axonal regeneration[15,16]. The second isolated molecule in MAIs, which is the most extensively studied molecule, is Nogo[17]. It consists of isoforms, Nogo-A, Nogo-B and Nogo-C. Among these, a structure called Nogo-66 is shared and serves as an inhibitory domain. Futhermore, Nogo-A has an additional inhibitory domain. Following these findings, the third inhibitory molecule called oligodendrocyte myelin glycoprotein (OMgp) was identified[18]. These three MAIs can bind to the Nogo-66 receptor (NgR) expressed in the neuronal membrane to initiate intracellular signaling transduction through RhoA[19–21].

Controversially, loss-of-function studies of MAIs *in vivo* generated conflicting results on their role in axon regeneration after CNS trauma[22]. For example, NgR−/− mice did not exhibit CST regeneration after spinal cord transection[23], possibly because chronic axon growth inhibition by myelin is mediated by an NgR-independent mechanism[24]. Another explanation of the controversy would be the variety of receptors for MAIs. It

has been explained by MAG-induced neuroprotective effect through gangliosides, another MAG receptor on axonal membranes[25,26]. The binding of MAG-gangliosides is likely to be sialic acid-dependent, because MAG is a lectin belonging to the sialic acid-binding immunoglobulin-like lectin family, whereas MAIs-NgR bindings are independent to sialic acid[27,28]. Moreover, MAG−/− mice have been shown to pass through progressive axon degeneration in the central and peripheral nervous system, resulting from elevated sensitivity to additional stress[29,30]. Therefore, the field lacks a cohesive mechanism on how to explain the MAIs-induced inhibitory signaling pathways.

1.3 Scar formation in injured CNS

Absence of axonal regeneration in the CNS has been causally related to the non-permissive nature of the glial environment surrounding regrowing axons; not only inhibitory signals from oligodendrocytes, but also secondary damages by inflammatory responses by activated microglial cells and reactive astrocytes. After CNS injury, inflammations in glial scar tissue initiate inhibitory influences on extension of mature

axons and, therefore, become a major obstacle to the subsequent processes of neuronal regeneration[1,2,7,31,32].

Blood brain barrier (BBB) disruption results in intrusion of non-CNS molecules into the brain parenchyma[33], leading to the formation of glial scar. The permeability change of BBB to blood and serum components lasts for up to 2 weeks after brain or spinal cord injury (SCI), and BBB breakdown accelerates activation and infiltration of macrophages/microglia[31]. Pro-inflammatory cytokine secreted from activated macrophages/microglia rapidly recruits astrocytes into the lesion site. Tips of non-regenerating axon become swollen. These dystrophic “endballs” are surrounded hypertrophic reactive astrocytes at injury core, leading to the hypothesis that the glial scar represents a physical wall. In fact, the glial scar does form a rubberlike and sticky growth-blocking membrane and inhibits axonal regeneration by the expression of the inhibitory extracellular matrix (ECM) components[2].

1.4 Inhibitors within the glial scar

In addition to CNS myelin, another important source of inhibitory molecules is the glial scar tissue. Here, two extensively investigated inhibitors are introduced: semaphorin3A (Sema3A) and chondroitin sulfate proteoglycan (CSPG).

Axon guidance is an important process in the neuronal development. The mechanisms of axon guidance can be divided into attractive and repulsive guidance. Sema3A is known to be secreted by glial cells majority being astrocytes or microglia[34]. The Sema3A functions have been implicated in a variety of neural wiring processes including axon guidance and bundling as well as neuronal migration via Plexin-A (Plex-A)-Neuropilin-1 (NP-1) complex expressed in plasma membrane of neurons[35]. Sema3A mRNA level is upregulated within glial scar after spinal cord injury[36]. Sema3A inhibits axonal regeneration in the CNS through repulsive reaction against growth cone of axon tip[37,38]. A selective inhibitor of Sema3A has been developed, but no extensive descending CST was observed in the spinal cord at locations within or far caudal to the lesion site in the inhibitor-administrated rats group[39]. Moreover, there are possible side effects in targeting Sema3A for SCI treatment as the embryonic lethality of

Sema3A-deficient mice infers[40,41], possibly because of its broad expression in neural tissues as well as in other organs such as developing lungs, bones and heart[41,42].

Proteoglycans have been implicated to act as barriers to CNS axon elongation by the facts that they control the guidance of the commissural and dorsal column axon pathways[43]. Astrocytes produce a class of proteoglycans[44], including CSPG[45]. The first piece of evidence which suggests a possible role of CSPG in the inadequate regeneration in the injured CNS was that CSPGs are secreted rapidly (within 24 hours) after injury and can persist for many months[46] in mature mammals. Upregulation of proteoglycans within the complex ECM produced by highly reactive mature astrocytes has been confirmed by a *in vitro* study[47]. Chondroitinase, an enzyme from the bacterium *Proteus vulgaris* that removes CSPG glycosaminoglycan (GAG) side chains from the protein core. Administration of chondroitinase to rodents with SCI degraded CSPG at the injury site allowed regeneration of small number of both ascending sensory and descending motor axons to pass the lesion, leading to locomotor and proprioceptive functional recovery[48,49]. However, limitations of regeneration with chondroitinase treatment have been reported. Multiple regions of proteoglycans can inhibit neurite

outgrowth[50]. As aggrecan predigested with chondroitinase still inhibits regeneration, thus undigested region with chondroitinase in CSPG may still inhibit axon elongation[51]. Therefore, other strategies that entirely remove the CSPG-mediated inhibitory signals are required.

1.5 Current therapeutic approaches for spinal cord injury

Most of tragic CNS diseases, such as Alzheimer's disease, Parkinson's disease, and even SCI, have lots of similarities in how neurons degenerate. CNS disorders involve immense axonal degeneration and long-lasting secondary damage on nervous system by inflammation. CNS manages to help the neurons with molecular defenses, but ultimately killing the neurons instead. No more than conservative therapy has been effective when a spinal cord is bruised or injured.

The spinal cord functions as the main motor and sensory pathways for connecting the brain and peripheral nervous system. The vertebrate spinal cord is divided into 31 segments. Injuries induce paraplegia below the injured level with lots of manifestations, such as hemiplegia, excretory disorder and dysfunction of thermoregulation. In

hospitals patients with SCI require substantial physical therapy and rehabilitation. However, these treatments are just aimed for maximizing the function of remained axons. A clinical study has shown that steroid methylprednisolone administration to inhibit the inflammatory responses within 8 hours after injury would be beneficial for SCI patients in the acute phase[52], however, it seemed to be effective for only young patients and the treatment is not generally applicable owing to side effects of high-dose steroid treatments. To achieve a complete recovery, substitute and/or compensatory therapeutic strategies based on molecular findings are thus still needed.

Although numerous molecular and cellular mechanisms have been found for CNS repair after traumatic injury as mentioned above, all the indicated extrinsic molecules have each problem. *In vivo* loss-of-function studies of MAIs still produce opposing results in axon regeneration after CNS trauma[22]. There are concerns of strong side effects when targeting Sema3A, as embryonic lethality of Sema3*A*-deficient mice indicates[40,41], possibly because of the broad requirement of it in neural tissues as well as in other organs as its broad expression in infers[41,42]. Digestion of CSPG with chondroitinase does not result in complete block of neurite outgrowth inhibition[51].

No target molecule that regulates both axonal growth and scarring has been identified, possibly because the field lacks a perspective on neuronal intrinsic mechanism[53]. In order to obtain effective regeneration with less side effects outside of nervous system by disrupting these inhibitory signals, this study focused on a common downstream molecule in among intracellular signals that is highly expressed in the nervous system.

1.6 Collapsin response mediator protein (CRMP)

Cytoskeletal dynamics is a key factor limiting the regenerative capacity of the CNS in terms of axon formation, inflammation, and scarring[21,54–58]. CRMP4 is one of the CRMP family proteins that is highly expressed in the developing and adult nervous system among vertebrates and regulates aspects of neurite growth by its binding to the cytoskeleton[59–64]. CRMP1-4 have high reciprocal homology (70-80%) and forms heterotetramers with the parts of the central dihydroorotase-like domain and C-terminal amino acid domain[65–67]. The C-terminal 80 amino acid domain (490-570) of CRMPs was identified as a crucial part for their binding to cytoskeleton[68,69]. Sema3A-induced Cdk5 phosphorylation of CRMP4 on the S522 residue and subsequent GSK3β phosphorylation on the S518, T514, T509 residues[68,70] decrease CRMP4 binding affinity

to tubulin heterodimer and F-actin, resulting in cytoskeletal depolymerization[71,72]. The CRMP4 allele produces short and long isoforms that are different in the length of their N-termini, which have been referred to as "a" (short) and "b" (long) isoforms, respectively[73,74]. This structural difference provides additional protein-protein interactions[75] (**Fig. 1.1**).

Previous studies have demonstrated that the long-form CRMP4 (CRMP4b)[74] is required for inhibitory responses to MAIs *in vitro*[75,76]. This suggests the possibility of involvement of CRMP4 in CSPG-induced signaling, because MAIs and CSPG inhibition share intracellular mechanisms through their common receptor NgR[77]. Moreover, injury-induced neuronal calpain activation produces a C-terminus-truncated form of CRMP4 (tCRMP4) that initiates neuronal cell death[78,79]. CRMP4 is therefore a common mediator of several inhibitory signaling pathways operating after traumatic injury (**Fig. 1.2**).

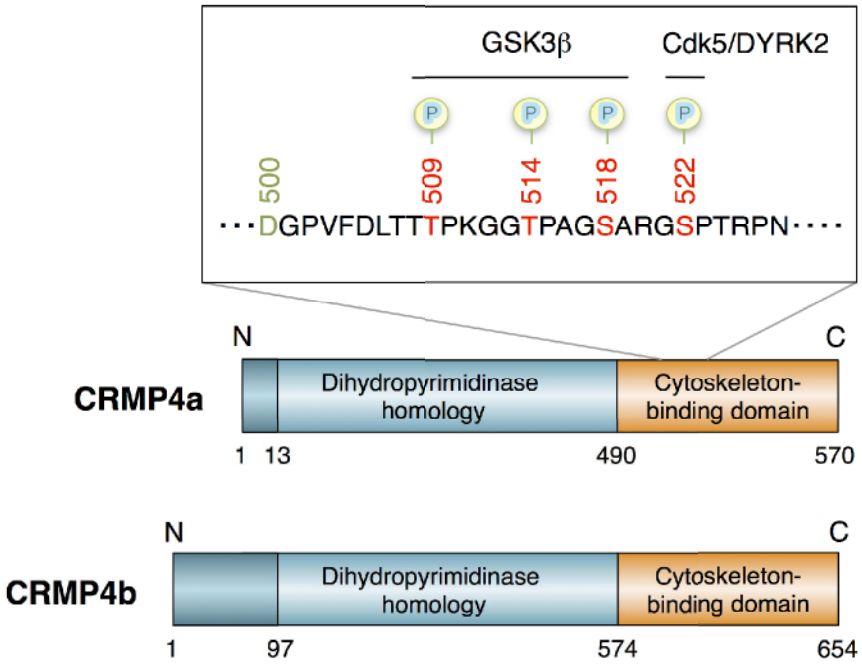

Fig. 1.1 Primary structure and domain organization of CRMP4. The short form of CRMP4 (CRMP4a) is polypeptides of 570 residues. Although CRMP shares sequence similarity with liver dihydropyrimidinase, purified brain CRMP does not hydrolyze several substrates of dihydropyrimidinase[65]. The C-terminal region (residues 490-570) is implicated to bind to cytoskeletal proteins[69]. Phosphorylations at several sites (red) by kinases control the binding affinity[68,70,75]. The long form of CRMP4 (CRMP4b) has a longer N-terminus[74] to interact with for other proteins, e.g. RhoA[75,76].

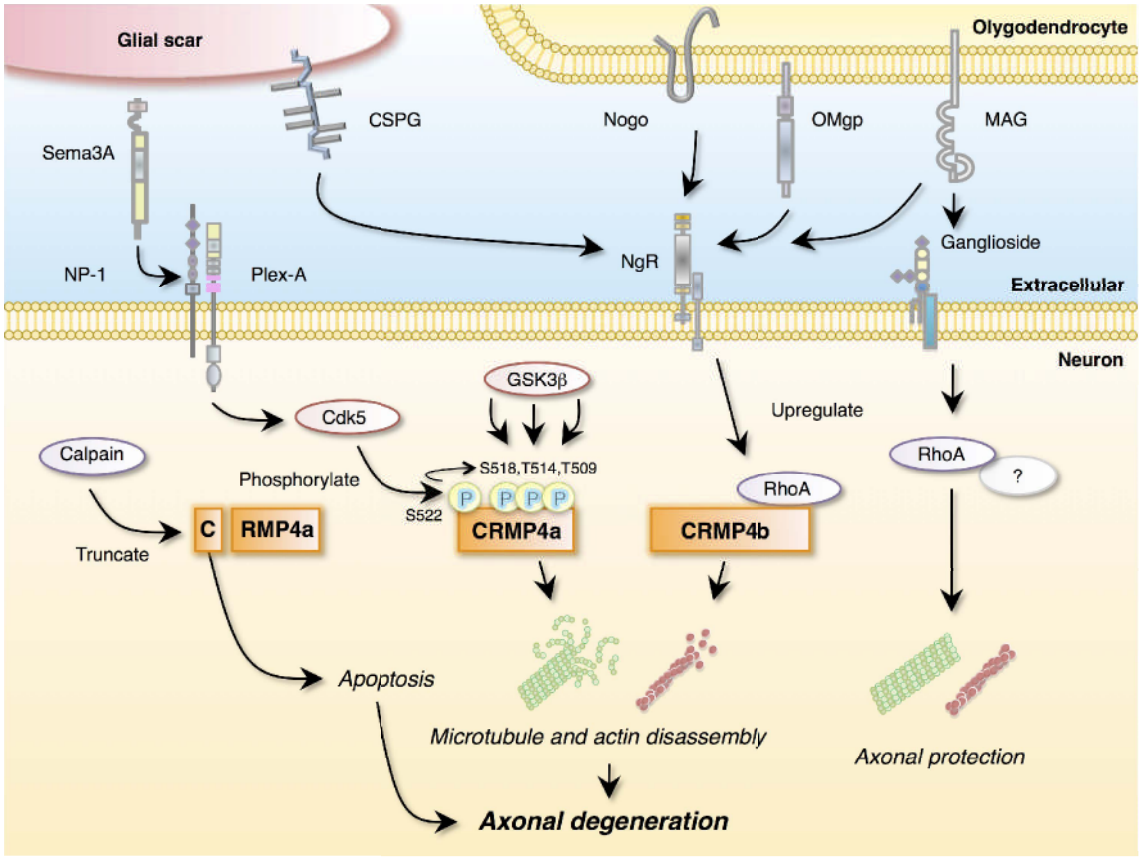

Fig. 1.2 Axonal outgrowth inhibitors of the adult CNS and intracellular signaling mechanisms regarding CRMP4. The glial scar secretes Sema3A and expresses CSPG. Sema3A binds to NP-1/Plex-A complex on the neuronal plasma membrane, and CSPG initiates intracellular signaling cascades through NgR that is a shared receptor with MAIs including Nogo, OMgp and MAG in the membrane of intact oligodendrocytes and myelin debris. The common downstream component among these extracellular inhibitors is CRMP4. Sema3A-mediated activations of cyclin-dependent kinase 5 (Cdk5) and glycogen synthase kinase 3 β (GSK3β) lead to CRMP4 phosphorylation. The signals via NgR upregulate the expression of CRMP4b, long form of CRMP4, to interact with RhoA. These two pathways are known to disrupt the polymerizations of microtubule and actin cytoskeleton. Activated calpain by the rise of intracellular calcium after injury truncates C-terminus of CRMP4 that is imported into nucleus to accelerate apoptosis. These signaling cascades induce continuous axonal degeneration, while MAG protects neurons against acute toxic insult through another ganglioside receptor and complex of RhoA with unknown molecule.

However, the involvement of CRMP4 in MAG-induced axonal protective effects remains unknown. Furthermore, the function of CRMP4 following traumatic CNS injury *in vivo* has never been examined. In this study, I first showed the involvement of CRMP4 both in MAG-induced axonal outgrowth inhibition and protection against acute toxic insult *in vitro* by using *Crmp4*–/– mice recently generated by our group[80]. Next, I characterized CRMP4 as a unique factor that is responsible for both axonal growth inhibition and scar formation after SCI. I found increases in phosphorylated CRMP4 (pCRMP4), CRMP4b, and tCRMP4 in injured spinal cord. The deletion of CRMP4 resulted in neuroprotective effects against SCI by suppressing depolymerization of microtubules, apoptosis, and demyelination. Notably, CRMP4 expression was upregulated in activated microglia/macrophages and reactive astrocytes after SCI, consistent with an observed reduction of inflammatory responses and scarring upon CRMP4 deletion. This permissive environment promoted axon growth in injured spinal cord and improved locomotion after SCI. My results suggest that inactivation of CRMP4 is a potential therapeutic strategy that addresses the two main obstacles against recovery after SCI.

Chapter 2. Materials and Methods

Animals

Mice used in the experiments were housed in accordance with the technical protocols for animal experiments approved by the Institutional Animal Care and Use Committee at Waseda University (2013-A085, 2014-A093). *Crmp4*−/− mice were generated and maintained in 129/Sv x C57BL/6J hybrid background as previously described[80]. The control *Crmp4*+/+ mice and *Crmp4*−/− mice were obtained by intercrossing *Crmp4*+/− mice and their offspring. YFP-H mice (Jackson laboratory, ME, USA)[81] were crossed with *Crmp4*−/− mice for the analysis of CST axons. All the experimenters were blinded to the genotype and treatment condition.

Axonal outgrowth assays

Axonal outgrowth assays were performed as described previously[21]. Plastic four well dishes (Thermo Scientific, 173740) were coated with 10 μg/mL laminin (Wako, 120-05751) for 1 hour (h) at room temperature (RT). Postnatal day (P) 3–8 dorsal root ganglion (DRG) neurons were dissociated and triturated with collagenase type III (Worthington, CLS-3) for 2 h and 0.25% trypsin/ ethylenediaminetetraacetic acid

(EDTA) (Sigma) for 15 minutes (min) at 37 degrees, and incubated in Ham's F-12 media (Gibco) with 10% fetal bovine serum (FBS) and 100 U/100 μg/mL penicillin/streptomycin (Wako). The cultures were stimulated with either 25 μg/mL MAG-Fc (R&D) or Fc control (R&D) at 24 hours after plating. 24 hours after the stimulation, fixation was conducted with 4% paraformaldehyde (PFA)/20% sucrose, followed by immunofluorescent staining with a monoclonal anti-neuronal βIII-tubulin antibody (mouse IgG, Tuj1, 1:1000, Covance, MMS-435P) and Alexa Fluor® 488-conjugated anti-mouse IgG (Invitrogen, A11008). Then, the cultures were mounted with Vectorshield Mounting Medium for Fluorescence with 4', 6-diamidino-2-phenylindole (DAPI) (Vector) and visualized with confocal microscopy (FV 1000, Olympus). For axonal outgrowth quantification, total length of axons from DRG neurons were measured using the MetaMorph image analysis (Universal Imaging Systems) as described previously[26]. Four–five random images derived from the four culture wells from three independent experiments were analyzed for each experimental condition.

Growth cone collapse assay

Glass coverslips (Fisher) were coated with 0.1% polyethylenimine (PEI) for overnight (O/N) and with 10 μg/mL laminin for 1 h. Postnatal 3–6 weeks DRG explants were put on coverslips with MEM medium (Nacalai Tesque) containing 5% FBS, 5% horse serum (HS), 2 mM L-glutamine (Gibco), and 100 U:100 μg/mL penicillin–streptomycin (Wako), followed by 50 ng/mL nerve growth factor (NGF) (Wako) administration 4–6 h later. At day *in vitro* (DIV) 3, the explants were stimulated by either MAG-Fc or Fc control (25 μg/mL, R&D) for 30 min and fixed with 4% PFA/20% sucrose. Axons from DRG neurons were stained with Alexa Fluor® 488 phalloidin (Invitrogen) and imaged by fluorescence microscopy (BX 51, Olympus). Nuclei were labeled using Vectorshield mouting media with DAPI (Vector). Growth cone collapse was identified by the morphological features of growth cones and scored as described previously[59].

Vincristine-induced axonal degeneration

Plastic coverslips (Nunc) were coated with 10 μg/mL laminin for 1 h. Postnatal 3–8 weeks DRG explants were cultured in Neurobasal medium (Invitrogen) with 10% FBS,

2% B27 (Invitrogen), 2 mM L-glutamine (Gibco), and 100 U:100 μg/mL penicillin–streptomycin (Wako). Indicated concentrations of Vincristine (VNC) (Sigma) dissolved in water were added to the culture at DIV 2 (defined as treatment day 0). At treatment day 3, images of DRG explants and their axons were captured under a phase-contrast microscope. For assessment of the neuroprotective effect of MAG against VNC, the cultures were co-stimulated with 20 nM VNC and either 25 μg/mL of MAG-Fc or Fc (R&D) at DIV 2. Images of DRG explants and their axons were captured under phase-contrast microscope after 72 h and the area of the DRG halo was quantified as described previously[82].

To examine detailed axonal degeneration of DRG neurons morphologically after VNC-induced toxic insult, dissociation culture was prepared as described above. At 24 h after administration of 20 nM VNC at DIV 2, the dissociated DRG neurons were fixed with 4% PFA/20% sucrose and immunostained with Tuj1 antibody (Covance, 1:1000) and Alexa Fluor® 488-conjugated anti-mouse IgG (Invitrogen, A11008), followed by mounting with VectorShield with DAPI (Vector) and visualizing with fluorescence microscopy (BX 51, Olympus). At least thirty DRG neurons were analyzed for

quantification of the percentage of intact axons in all axons in each condition.

Surgical procedures

All surgical procedures and postoperative care were performed in accordance with guidelines of Waseda University. Mice (6–9 weeks old) were utilized for all experiments. Mice were deeply anesthetized with 2-4% isoflurane (DS Pharma Animal Health) using an inhalation anesthesia apparatus (KN-1071 NARCOBIT-E (II), Natsume Seisakusho). Laminectomies were performed at the 7-8th thoracic spinal cord levels (T7-T8), exposing the spinal cord. A 1.5-mm-deep near-complete dorsal transection was performed at T7-T8 using a pair of microscissors (NAPOX® MB-50-15, Natsume Seisakusho) and the tip of a 28-gauge needle to sever dorsal white matter, all the gray matter, the 5-HT-positive raphespinal tract, and the main dorsal CST axons. The skin on the back was closed with a nylon stitch (USP4-0, JIS No. 2, Natsume Seisakusho). After the operation, the mice were kept warm, placed on beds of sawdust, and given manual bladder evacuation once per day. Food was provided on the cage floor, and the mice had no difficulty in accessing water. Mice that showed 0-1 points of BMS score at 1 day after SCI were used for the following experiments and analyses.

Microinjections

Non-traumatic intraspinal microinjection of Zymosan A was performed as previously described[83]. Briefly, 50 nL Zymosan A (12.5 mg/ml, 273-01491, Wako) was injected into the lateral funiculi of spinal cords 1–1.2 mm lateral to the spinal cord midline and at 0.5–0.7 mm depth at the level of T7/8. Injections were carried out over 5 min using calibrated pressure ejection (Harvard Apparatus, Pump 11 Elite Syringe Pumps). Mice were sacrificed 3 days after injection and then analyzed.

Immunoblotting

The tissue sampling and western blotting were performed as previously described[39,84] with some modifications. A spinal cord tissue block of 3-mm length centered at the injury site or Zymosan A injection site were dissected out at 2 and 24 h after SCI from male and female WT C57BL/6J mice, and at 1, 2, 3, 4 and 14 weeks after SCI from female WT C57BL/6J mice. The same potion of the spinal cord was dissected out from intact female WT C57BL/6J mice (n = 3 mice for each time point). The tissue samples were homogenized in lysis buffer [20 mM Tris-HCl, 150 mM NaCl, 1 mM EDTA, 10 mM NaF, 1 mM Na_3VO_4, 1% Nonidet P-40, proteinase inhibitor (Complete proteinase

inhibitor cocktail, 11 873 580 001, Roche, one tablet in 50 ml lysis buffer), and phosphatase inhibitor (PhosphoStop, 04 906 845 001, Roche, one tablet in 10 ml lysis buffer)] as previously described[84]. The homogenates were centrifuged at 1,200 rpm for 15 min at 4 degrees. The supernatants were assayed for protein concentration using Bio-Rad Protein Assay Dye Reagent Concentrate (500-0006, Bio-Rad Laboratories) and a spectrophotometer (Gene Quant 1300, GE Healthcare). The proteins were separated on 12.5% or 15% sodium dodecyl sulfate (SDS)-PAGE gels and then transferred to Immobilon®-P Transfer Membranes (IPVH07850, Millipore). After the transfer, the membranes were placed in Tris-buffered saline (TBS) with 0.05% Polyoxyethylene (20) Sorbitan Monolaurate (Tween 20) (166-21115, Wako) (0.05% TBST) containing 3% bovine serum albumin (BSA) (A7906, Sigma-Aldrich) for O/N at 4 degrees to block nonspecific binding. The blots were incubated for 1h with following primary antibodies: anti-CRMP4 (rabbit IgG, 1:1000, AB5454, Millipore), anti-CRMP4b (rabbit IgG, kindly provided by Dr. Quinn [McGill University]), anti-phosphorylated (at Ser 522) CRMP4 (rabbit IgG, 1:1000)[80], anti-α-tubulin (rabbit IgG, 1:1000, T6199, Sigma-Aldrich), anti-GAP43 (rabbit IgG, 1:1000, ab16053, Abcam), anti-β-tubulin

(rabbit IgG, 1:1000, T8328, Sigma-Aldrich), or anti-TNFα (rabbit IgG, AB2148P, Millipore), diluted in blocking buffer at RT. The membranes were then washed in 0.05% TBST for 10 min for three times and incubated with horseradish peroxidase-conjugated anti-mouse or anti-rabbit IgG (1:10,000, sc-2005 or sc-2004, Santa Cruz Biotechnology) at RT for 1 h. After washing in 0.05% TBST for 10 min for three times, the membranes were developed using a color substrate (Pierce® Western Blotting Substrate Plus, NCI32132JP, Thermo Fisher Scientific). The reaction was stopped by washing each membrane with TBS. Tubulin was detected in parallel as loading controls. The membranes were scanned with a Luminescent Image Analyzer (LAS-3000, Fujifilm), and the resulting digital images were quantified and normalized relative to tubulin level for each sample using the ImageJ software (Rasband, W.S., ImageJ, U. S. National Institutes of Health, Bethesda, Maryland, USA, http://imagej.nih.gov/ij/, 1997-2014).

Immunohistochemistry

The mice were perfused with ice-cold 4% paraformaldehyde/0.1M phosphate-buffered saline (pH 7.4) (PBS) solution. A 15-mm length of spinal cord part centered on the

injury site or Zymosan A injection site was dissected out and postfixed O/N in the same fixative. Then the spinal cord was soaked in a succession of solutions at 4 degrees O/N (PBS, 10% sucrose and 20% sucrose, respectively) and embedded in a 2:1 mixture of Tissue Tek® optimal cutting temperature (OCT) compound (4583, Sakura Finetek) and 20% sucrose for cryostat sectioning (30 μm) on a Cryostat (CM1860, Leica). The sections were mounted on MAS-coated slide glasses (S9441, Matsunami) and stored at -20 degrees until further analysis. Immunofluorescence staining was performed as previously described[84]. Prior to staining, tissue sections were dried in air for 1 h and washed in PBS for 30 min followed by permeabilizing and blocking with 3% normal horse serum (HS, S-2000, Vector Laboratories) diluted with 0.1% Polyoxyethylene (10) Octylphenyl Esther (Triton X-100, 169-21105, Wako)/PBS (PBST) for 1 h. Incubation at 4 degrees O/N was carried out with the following primary antibodies; anti-CRMP4 (rabbit IgG, 1:200, AB5454, Millipore), anti-MAP2 (mouse IgG, 1:200, MAB3418, Millipore), anti-detyrosinated α-tubulin (Glu-tubulin) (mouse IgG, 1:500, ab24622, Abcam), anti-neuron-specific class III β-tubulin (Tuj1, rabbit IgG, 1:1000, MMS-435P, Covance), anti-GFAP (mouse IgG, 1:400, G3893, Sigma-Aldrich), anti-OX-41 (mouse

IgG, 1:200, MAB1407P, Millipore), anti-Iba1 (rabbit IgG, 1:500, 019-19741, Wako) or anti-GFAP (rabbit IgG, 1:500, Z0334, Dako) antibody. After being washed in 0.01% PBST (10 min for three times), sections were incubated with secondary antibodies [Alexa Fluor® 488 or 568 goat anti-rabbit IgG (H+L) or Alexa Fluor® 594 goat anti-mouse IgG (H+L), 1:1000, A11008, A11011, A11005, Invitrogen, and NeuroTrace® 530/615 red fluorescent Nissl stain, 1:250, N-21482, Molecular Probes] in 0.01% PBST for 1 h at RT. Finally, the slides were washed for 10 min for three times in 0.01% PBST and once in PBS for 1 min before being dried and coverslipped. For immunostaining with anti-GAP43 (rabbit IgG, 1:200, ab16053, Abcam), or anti-collagen IV antibody (1:200, ab19808, Abcam), the sections were blocked with 5% HS in PBS for 1 h and permeabilized with 0.2% Tween 20 in PBS for 5 min for four times and 5% HS in 0.1% PBST for 1 h. For immunostaining with anti-5-HT (rabbit IgG, 1:4000, 20080, Immunostar), tissue sections were washed in high-salt buffer (HSB; 500 mM NaCl, 9.2 mM NaH_2PO_4, 12.5 mM Na_2HPO_4) for 10 min for three times and blocked with 5% HS diluted with 0.3% Triton X-100 in HSB. After the primary and secondary antibody reactions, the slides were washed for 10 min for three times with

HSB. Terminal deoxynucleotidyl transferase (TdT)-mediated deoxyuridine triphosphate-biotin nick end labeling (TUNEL) using Apop Tag Red (S7165, Millipore) was performed to detect apoptotic cells in the transected spinal cord by following manufacturer's protocol. FluoroMyelin™ Red Fluorescent Myelin Stain (F34652, Molecular Probes) was used to reveal myelin distributions in the transected spinal cord by following manufacturer's protocol. Nuclear staining was also performed with anti-fade mounting media VectorShield with DAPI (Vector). Images were visualized using microscopy (BX51, Olympus and BZ 8100, Keyence) and confocal fluorescence microscopy (FV-1000, Olympus).

Quantification for immunohistochemistry

To analyze Glu-tubulin distribution in the axon, I measured the length of Glu-tubulin-positive and Tuj1-positive fibers in each section of the spinal cords as previously described in detail[19]. Briefly, the area of dorsal white matter in the rostral and caudal stump, ~3 mm rostrally from the injury site, was examined. Average length of a subset of fibers was calculated, and the data was normalized to that of control. For each experimental condition, four random images from each of the three independent

sections from three mice were captured and 45 axons per mouse were analyzed. The lesion volume was delineated by its bounding surface, which is defined by a series of closed contours in the serial sections. For the quantification, at least 3 serial cross sections taken every 300 μm or serial parasagittal sections taken every 180 μm from 3 mice were analyzed as previously described[85] with some modifications. The areas of the microglial and astroglial activation, collagen IV-positive scar and the immunoreactivity of GFAP and 5-HT was quantified with ImageJ software (Rasband, W.S., ImageJ, U. S. National Institutes of Health, Bethesda, Maryland, USA, http://imagej.nih.gov/ij/, 1997-2014.). For analysis of inflammatory responses after SCI, images of cross sections at 1.5 mm caudal to the lesion site were analyzed. Zymosan A-induced inflammatory responses were examined 750 μm rostral and caudal to the injection site. Counts of the numbers of TUNEL-positive apoptotic cells with DAPI-positive nuclei were performed within 2.5 mm rostral and 2.5 mm caudal areas to the epicenter of injury. Quantification of 5-HT immunoreactivity was analyzed at 1-2 mm caudal to lesion epicenter of parasagittal sections.

Behavioral analysis

Hindlimb motor function was evaluated 1, 3, 5, 7, 14, 21 and 28 days after injury (n = 7 per group) using the locomotor rating of the Basso Mouse Scale (BMS) as previously described in detail[86]. This scale ranges from 0, indicating complete paralysis, to 9, indicating normal movement of the hindlimbs. A team of two experienced examiners evaluated each animal for 3-5 min and assigned a score based on a defined method where performance of the left and right hindlimbs was averaged.

Statistical analysis

Statistical differences between two groups were calculated with an unpaired two-tailed Student's *t* test. Other analyses were performed using two-way analysis of variance (ANOVA) with Dunnett's or Tukey's *post hoc* multiple-comparison test as appropriate to the design. The variance similarity between two samples was confirmed using F-test. All analyses were conducted using GraphPad Prism software version 6.0b. All data represent mean ± S.E.M.

Chapter 3. Results

3.1 The role of CRMP4 in MAG-induced signaling pathways *in vitro* (Nagai *et al*., 2012)

CRMP4 mediation of MAG-induced inhibitory response in cultured DRG neurons

In this study, I examined the role of CRMP4 in axonal regeneration/sprouting and degeneration. It has been shown that neurite growth inhibition of cultured neurons by myelin substrates is decreased with siRNA-mediated knockdown of CRMP4[75,76]. However, the siRNA did not completely reduce the gene expression of CRMP4[76] and there would be concerns about a potential off-target effect with RNA interference[87]. To determine whether or not CRMP4 is required for MAIs-induced axonal outgrowth inhibition via NgR, I took advantage of *Crmp4*−/− mice[80] where CRMP4 protein expression was specifically and totally eliminated. To examine the involvement of CRMP4 in axonal inhibitory response, DRG neurons derived from *Crmp4*−/− mice and *Crmp4*+/+ control mice were stimulated with soluble MAG-Fc for 24 hours. In the DRG neurons from the control mice, axon growth was 37.0±5.81% reduced in the

presence of 25 μg/mL MAG ($P < 0.01$). In contrast, the inhibitory effect of MAG was suppressed to 14.6±12.0% in *Crmp4*−/− DRG neurons (**Fig. 3.1.1a,b**). It has also been demonstrated that CRMP4b-RhoA complex might regulate growth cone collapse by modifying actin-based mechanism during myelin-mediated axon growth inhibition[76]. To examine the role of CRMP4 in MAIs-induced collapse of growth cone, axon tips of cultured DRG explants were assessed 30 min after MAG-Fc stimulation. There was no difference in the morphological features of the growth cones between *Crmp4*+/+ and *Crmp4*−/− DRG neurons without stimulation (**Fig. 3.1.1c**). While 53.7±2.44% growth cones from the *Crmp4*+/+ DRG neurons were collapsed by 25 μg/mL MAG-Fc ($P <$ 0.01), the ratio of MAG-Fc-mediated growth cone collapse was reduced to 31.9± 3.31% in the *Crmp4*−/− DRG neurons (**Fig. 3.1.1d)**. These results clearly confirmed that CRMP4 is required for MAG-induced inhibition of axon growth and growth cone collapse.

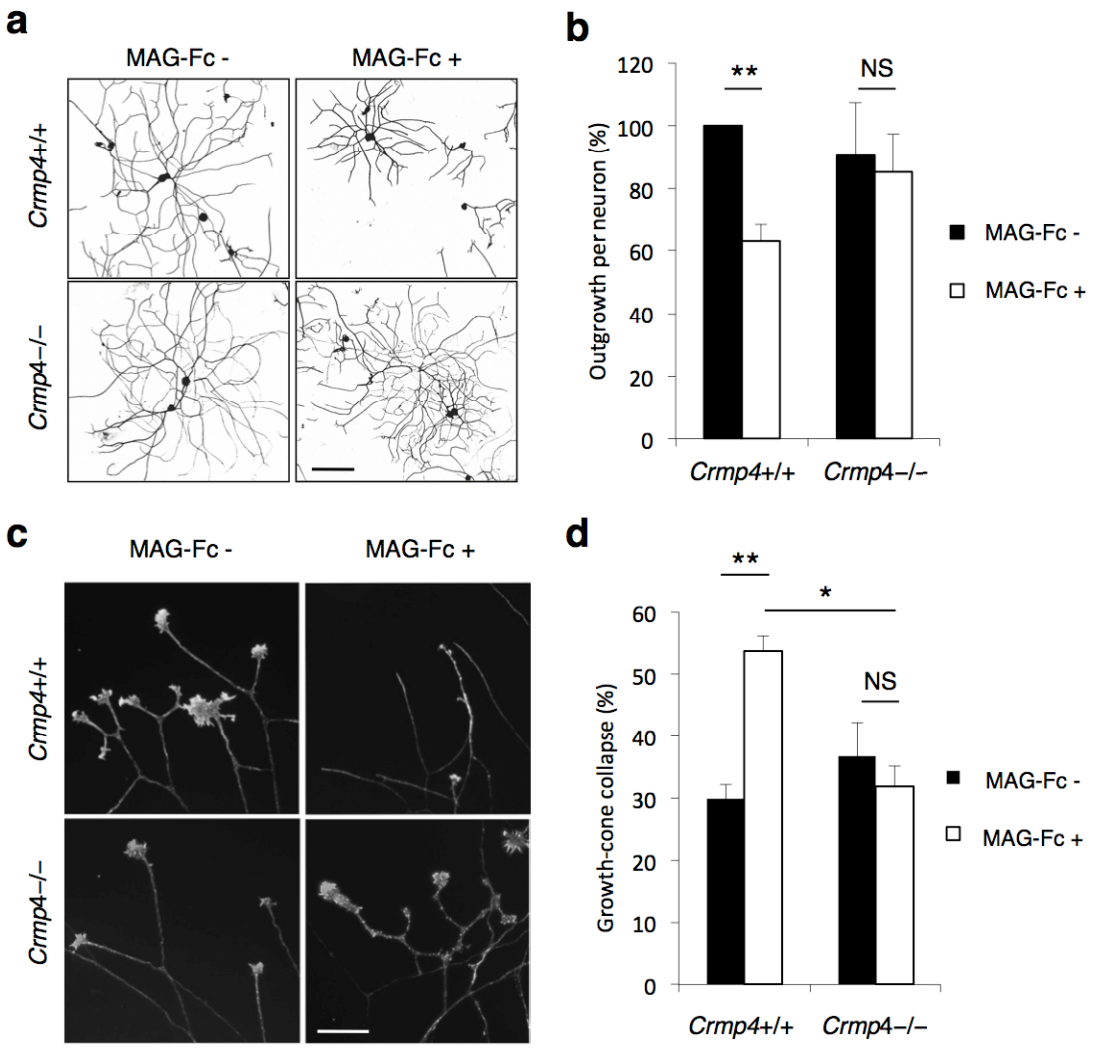

Fig. 3.1.1 Knockout of *Crmp4* reduced MAG-induced axon growth inhibition and growth cone collapse. (**a,b**) Axonal outgrowth assay of dissociated DRG neurons from P3–8 *Crmp4*+/+ and *Crmp4*−/− mice stained with Tuj1 antibody stimulated by 25 μg/mL MAG-Fc. n = 100–170 DRG neurons from 3 independent experiments. (**c**) Growth cone morphologies in *Crmp4*+/+ and *Crmp4*−/− dorsal root axons from postnatal 3–6 weeks stimulated by 25 μg/mL MAG-Fc were visualized with Alexa Fluor 488 phalloidin. (**d**) Ratio of growth cone collapse was quantified at least 100 growth cones of dorsal root axons from 3 independent experiments per each condition. Scale bars: 100 μm in **a** and 50 μm in **c**. Statistical analyses were performed using two-way ANOVA followed by Tukey's test. *, $P < 0.05$. **, $P < 0.01$. NS, no significant difference. Data represent mean ± S.E.M. (Nagai et al., 2012)

Crmp4 deletion elevates sensitivity to VNC-mediated axonal degeneration

A previous study has shown that short-form CRMP4 binds and stabilizes microtubule polymerization in neurons[71]. To determine the role of CRMP4 in axonal viability after acute toxic insult, I administrated an inhibitor of microtubule assembly, VNC[82], to cultured *Crmp4*+/+ and *Crmp4*−/− DRG neurons. I observed that the VNC exposure induced beading and segmented axons from the distal parts, leading to gradual decrease of DRG halo areas in both genotypes (**Fig. 3.1.2a**) as described previously[82]. The area of DRG halo of *Crmp4*+/+ dorsal root explants was reduced more rapidly with higher dose (>20 nM) of VNC at 72 h after VNC exposure when compared to that at treatment day 0 (0 h), indicating that the reduction in halo areas was dose-dependent in *Crmp4*+/+ DRG explants (**Fig. 3.1.2c**). However, severer degenerations were induced by lower VNC doses (5 and 10 nM) in the *Crmp4*−/− DRG neurons when compared to controls ($P < 0.05$ at 5 nM VNC treatment, **Fig. 3.1.2c**). To analyze the detailed morphology, immunocytochemical analysis of dissociated DRG neurons was performed. Tuj1 staining revealed that gradual increase in number of beading axons along with increase of VNC doses in *Crmp4*+/+ neurons (**Fig. 3.1.2b**). Compared with control

neurons, *Crmp4*−/− neurons showed significantly decreased ratio of non-beading intact axons when treated with 5 nM VNC ($P < 0.001$, **Fig. 3.1.2d**). These findings demonstrated that deletion of CRMP4 enhanced vulnerability to VNC in cultured DRG neurons.

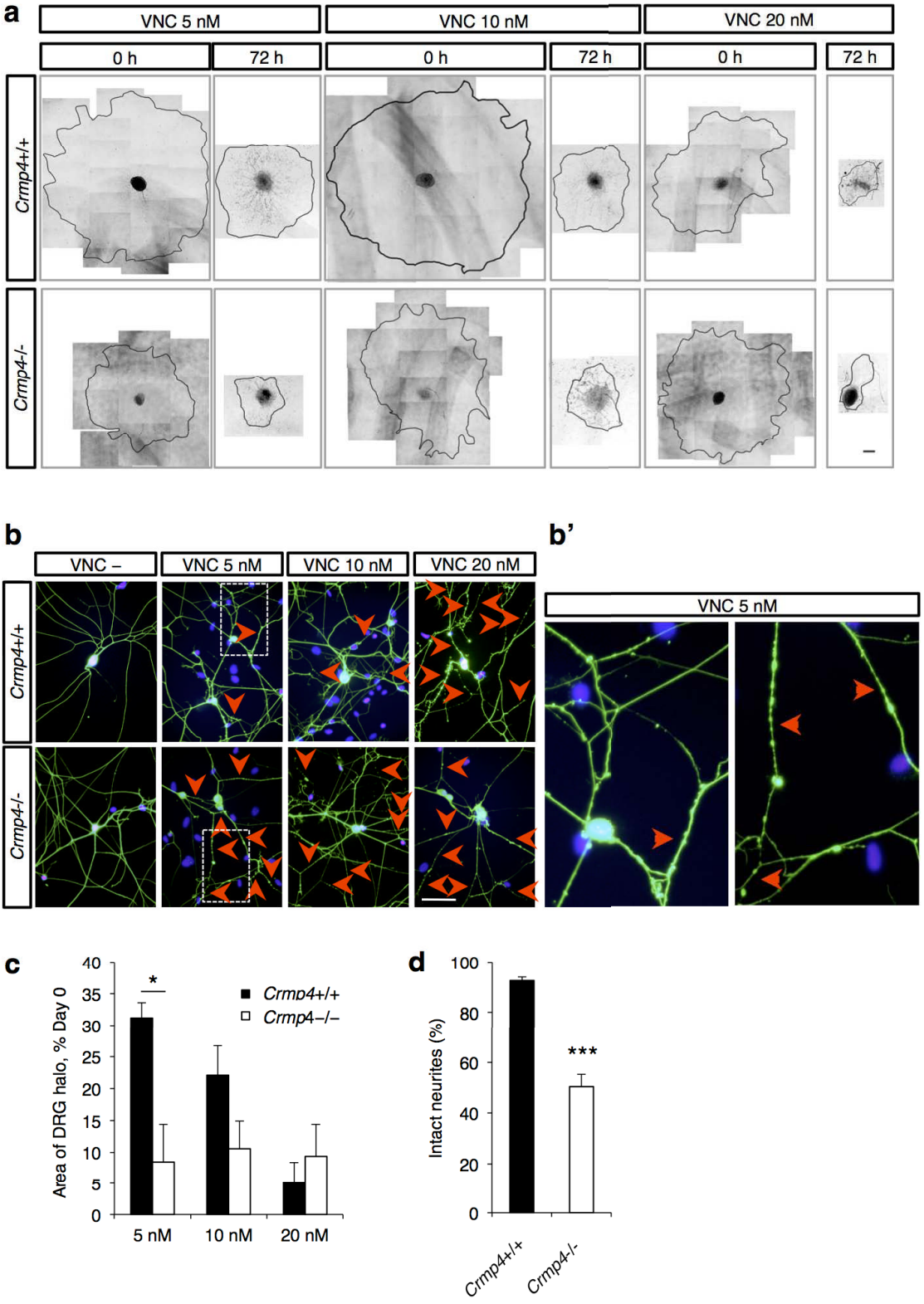
a
VNC 5 nM
VNC 10 nM
VNC 20 nM
0 h
72 h
0 h
72 h
0 h
72 h
Crmp4+/+
Crmp4-/-
b
VNC –
VNC 5 nM
VNC 10 nM
VNC 20 nM
Crmp4+/+
Crmp4-/-
b'
VNC 5 nM
c
Area of DRG halo, % Day 0
40
35
30
25
20
15
10
5
0
*
Crmp4+/+
Crmp4–/–
5 nM
10 nM
20 nM
d
Intact neurites (%)
100
80
60
40
20
0
***
Crmp4+/+
Crmp4-/-

Fig. 3.1.2

Fig. 3.1.2 Enhanced sensitivity to VNC-induced axonal degeneration in CRMP4−/− DRG neurons. (**a**) Phase-contrast images of DRG explants and their halo (circled with solid lines) after 0 h and 72 h treatment to 5, 10, and 20 nM VNC. (**b**) Dissociated DRG neurons from *Crmp4*+/+ and *Crmp4*−/− mice treated with VNC were labeled with Tuj1 antibody (green) and DAPI (blue). Note that neurons have degenerating axons (red arrowheads) still maintain intact nuclear morphology. Magnified images of boxed area in **b** are shown in **b'**. (**c**) Ratio of the area of the DRG halo after 72 h VNC exposure to that at treatment day 0 (n = 5–6 DRG explants). (**d**) Ratio of intact axons to all the axons of dissociated DRG neurons treated with 5 nM VNC. (n = 30–35 neurons). Scale bars: 200 μm in **a**, 50 μm in **b**. Statistical analyses were performed using an unpaired Student's *t* test. *, $P < 0.05$, ***, $P < 0.001$. Data represent mean ± S.E.M. (Nagai et al., 2012)

Axonal protection of MAG against VNC treatment is reduced in cultured CRMP4-null DRG neurons

MAG has a protective effect on neurons against acute toxic insult via gangliosides[25,26]. To examine the involvement of CRMP4 in MAG-induced axonal protection signal transduction, cultured *Crmp4*+/+ and *Crmp4*−/− DRG explants were incubated with 25 μg/mL MAG-Fc and 20 nM VNC. The area of DRG halo of *Crmp4*+/+ dorsal root explants was reduced to 3.11±1.97% after 72 h VNC exposure when compared to that at treatment day 0. 18.5±5.20% area of DRG halo was observed after 72 h incubation with VNC and MAG-Fc, suggesting the axonal protection with MAG-Fc (**Fig. 3.1.3a,b**). This axonal protective effect of MAG was confirmed by the experiment with Fc control, where I observed no significant difference in DRG halo area between DRG explants with VNC and with VNC+Fc control stimulations (**Fig. 3.1.3c**). Conversely, *Crmp4*−/− DRG axons were almost completely degenerated with the VNC treatment regardless of MAG-Fc presence (5.51±5.51% and 4.18±3.00% area of DRG halo when compared to those at treatment day 0, without MAG and with MAG, respectively), indicating that the MAG-mediated protective effect on cultured neurons disappeared upon *Crmp4*

deletion ($P < 0.05$, **Fig. 3.1.3b**). This data suggested that CRMP4 is required for MAG-mediated axonal protection.

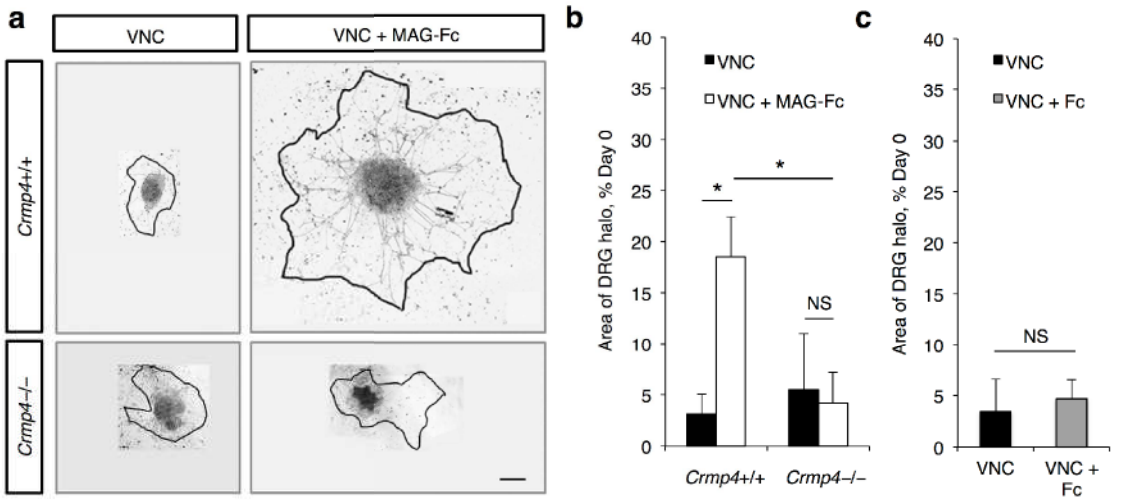

Fig. 3.1.3 Suppressed axonal protective effect of MAG against VNC in the cultured *Crmp4–/–* DRG neurons. (**a**) Phase-contrast images of DRG explants from *Crmp4*+/+ and *Crmp4–/–* mice after 72 h treatment of 20 nM VNC with or without 25 μg/mL MAG-Fc. Although MAG-induced axonal protection against VNC was observed in the *Crmp4*+/+ explants, *Crmp4–/–* DRG neurons exhibited axonal degeneration after VNC treatment in the presence of MAG. (**b,c**) Ratio of the area of the DRG halo after 72 h VNC exposure to that at treatment day 0 (n = 3 DRG explants). In *Crmp4*+/+ DRG neurons, MAG-Fc stimulation suppressed the decrease in area of DRG halo by VNC (**b**), whereas the suppression of axonal degeneration was not observed with Fc control stimulation (**c**). Scale bar: 200 μm in **a**. Statistical analysis was performed using two-way ANOVA followed by Tukey's test. *, $P < 0.05$. NS, no significant difference. Data represent mean ± S.E.M. (Nagai et al., 2012)□

3.2 The role of CRMP4 in recovery after spinal cord injury *in vivo* (Nagai *et al*., 2015)

Increased expression levels of CRMP4 after SCI

Given the role of CRMP4 as a mediator of MAIs *in vitro*, I next examined the role of CRMP4 in regenerative and/or degenerative responses after CNS traumatic injury *in vivo*. I first analyzed the change of CRMP4 protein expression after dorsal transection of the mouse spinal cord. To examine the temporal changes in the protein levels of CRMP4 and its phosphorylated and truncated forms after SCI, I performed immunoblotting of the spinal cord tissues at several time points post SCI. I detected three bands around the 65-kDa CRMP4a isoform with anti-CRMP4 antibody (**Fig. 3.2.1a**). The total amount of CRMP4a was increased in injured spinal cords (**Fig. 3.2.1d**). The bottom of three bands recognized as 58-kDa tCRMP4 (**Fig. 3.2.1a**; solid arrow) was upregulated after transection (**Fig. 3.2.1e**). The top of three bands seemed a part of pCRMP4 (**Fig. 3.2.1a**; solid arrowhead) as phosphorylation of CRMPs induces band shifts in SDS-PAGE[80,88]. The specific antibody for phosphorylated CRMP4 on the Ser522 residue revealed pCRMP4 was included within all the three bands (**Fig. 3.2.1b**)

and the pCRMP4S522 level was enhanced at both the acute and the sub-chronic phases of injury (**Fig. 3.2.1f**). Moreover, the 75-kDa isoform of CRMP4 was identified as CRMP4b using a specific antibody (**Fig. 3.2.1c**). Levels of CRMP4b were distinctly higher in injured spinal cords, peaking 1 to 2 weeks post SCI (**Fig. 3.2.1a,g**). These results indicate that forms of CRMP4 that are toxic or inhibitory to axonal growth were induced by SCI with a unique time course.

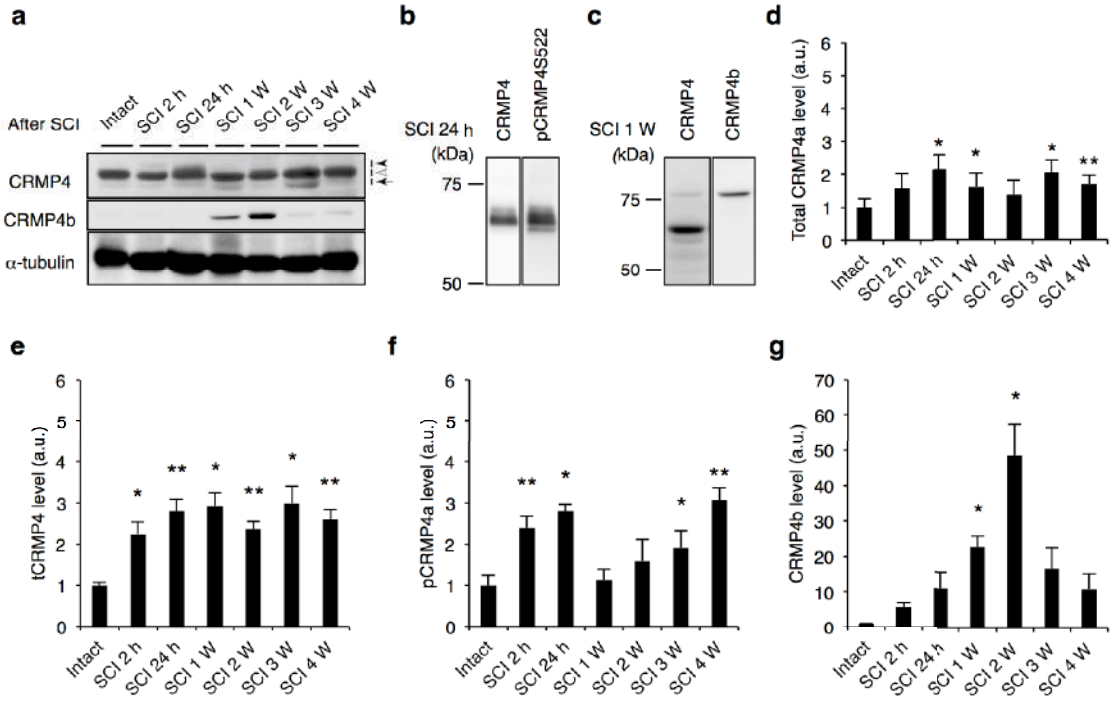

Figure 3.2.1 Change of CRMP4 expression level after SCI. (**a**) Immunoblot analysis of CRMP4 levels in intact and injured spinal cords from wild-type mice with anti-CRMP4 and anti-CRMP4b antibodies. Anti-CRMP4 antibody detected a part of phosphorylated CRMP4a (solid arrowhead), tCRMP4a (solid arrow) around the band of 65-kDa CRMP4a (open arrowhead). (**b**-**c**) Band patterns with anti-CRMP4 antibody and with the antibody for phosphorylated CRMP4 at Ser522 residue (pCRMP4S522) (**b**) and with anti-CRMP4 and anti-CRMP4b antibodies (**c**). (**d-g**) Quantitative analysis of different forms of CRMP4. *, $P < 0.05$, **, $P < 0.01$. compared with the intact spinal cord. n = 5 mice at each time-point. Statistical analysis was performed using one-way ANOVA followed by Dunnett's test. Data are mean ± S.E.M. h, hours; W, weeks. (Nagai et al., 2015)

Next, I examined which cell types expressed CRMP4 after SCI. A markedly increased CRMP4 expression level has been reported in spinal motoneurons in a mutant SOD1 mouse model[89] and in adult sensory neurons after sciatic nerve injury[90]. I first conducted double immunostaining for a neuronal marker and CRMP4 in cross sections of spinal cords. I detected CRMP4 expression and found that it was localized with Nissl-positive cell bodies of motoneurons and MAP2-positive their dendrites in the ventral horn of intact and injured spinal cords (**Fig. 3.2.2a,b**). The level of CRMP4 in positive neurons was significantly above background seen in *Crmp4*−/− spinal cords (**Fig. 3.2.2a**). While CRMP4 was evident in Nissl-positive neuronal cell bodies both intact and injured spinal cords, its expression in neurites around somata (e.g. MAP2-positive dendrites) was increased after lesion. However, it is possible that the protein level of CRMP4 is upregulated not in neuron but in other cell types, such as inflammatory cells. To analyze CRMP4 protein expression in microglia/macrophages and reactive astrocytes before, during, and after inflammatory responses to SCI, I double immunostained parasagittal sections of spinal cords for CRMP4 and glial fibrillary acidic protein (GFAP), a marker for normal as well as reactive astrocytes, or

OX-41, a marker for microglia/macrophages[91]. The CRMP4 staining signal was weak in both GFAP-positive and OX-41-positive cells in the gray matter of intact spinal cord (**Fig. 3.2.2c,d**; open arrowheads). However, CRMP4 immunoreactivity was remarkably enhanced in both types of glial cells adjacent to the lesion site and in the astroglial scar after SCI (**Fig. 3.2.2c,d**; solid arrowheads).

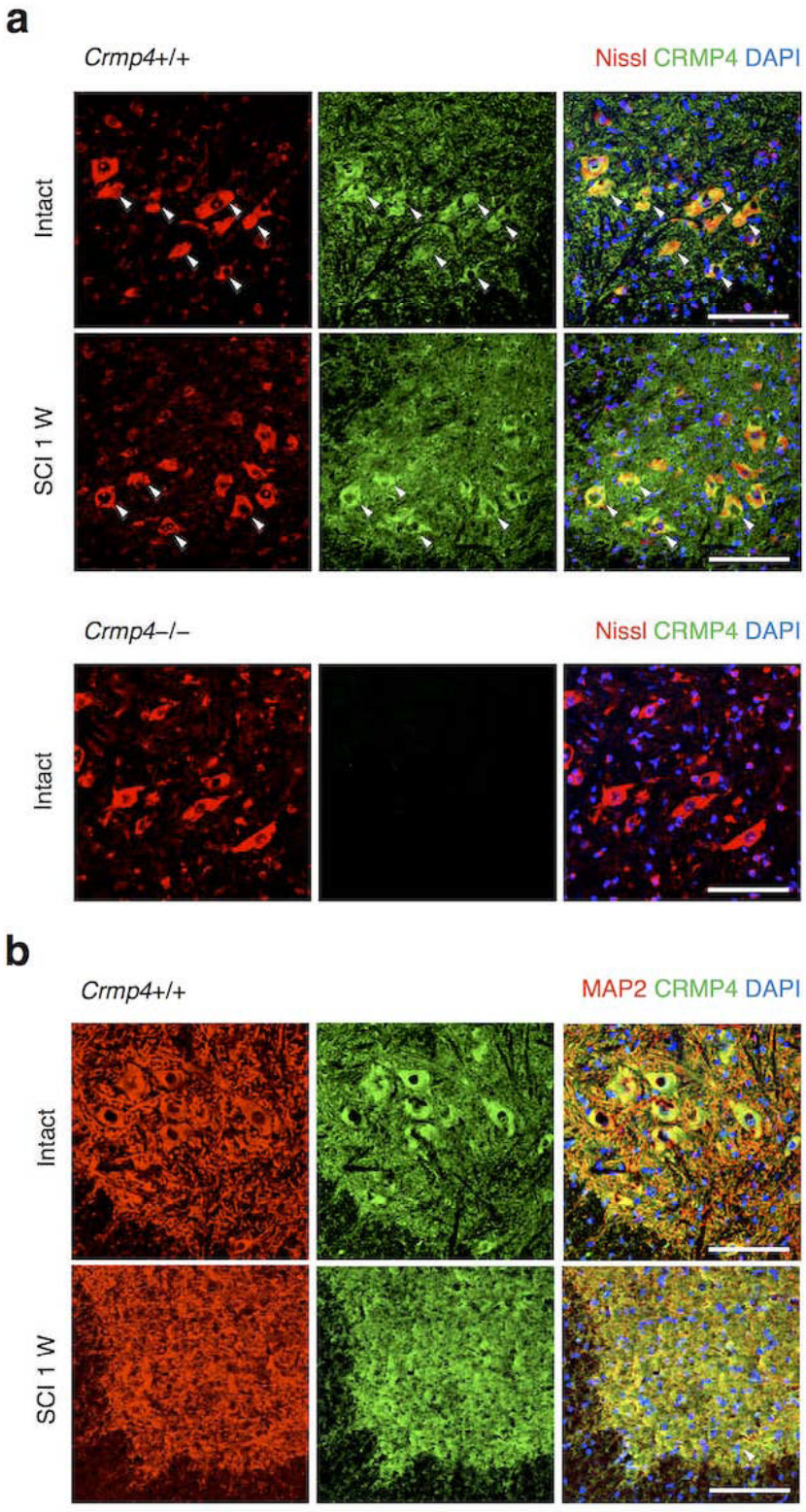
a
Crmp4+/+
Nissl CRMP4 DAPI
Intact
SCI 1 W
Crmp4−/−
Nissl CRMP4 DAPI
Intact
b
Crmp4+/+
MAP2 CRMP4 DAPI
Intact
SCI 1 W

Figure 3.2.2

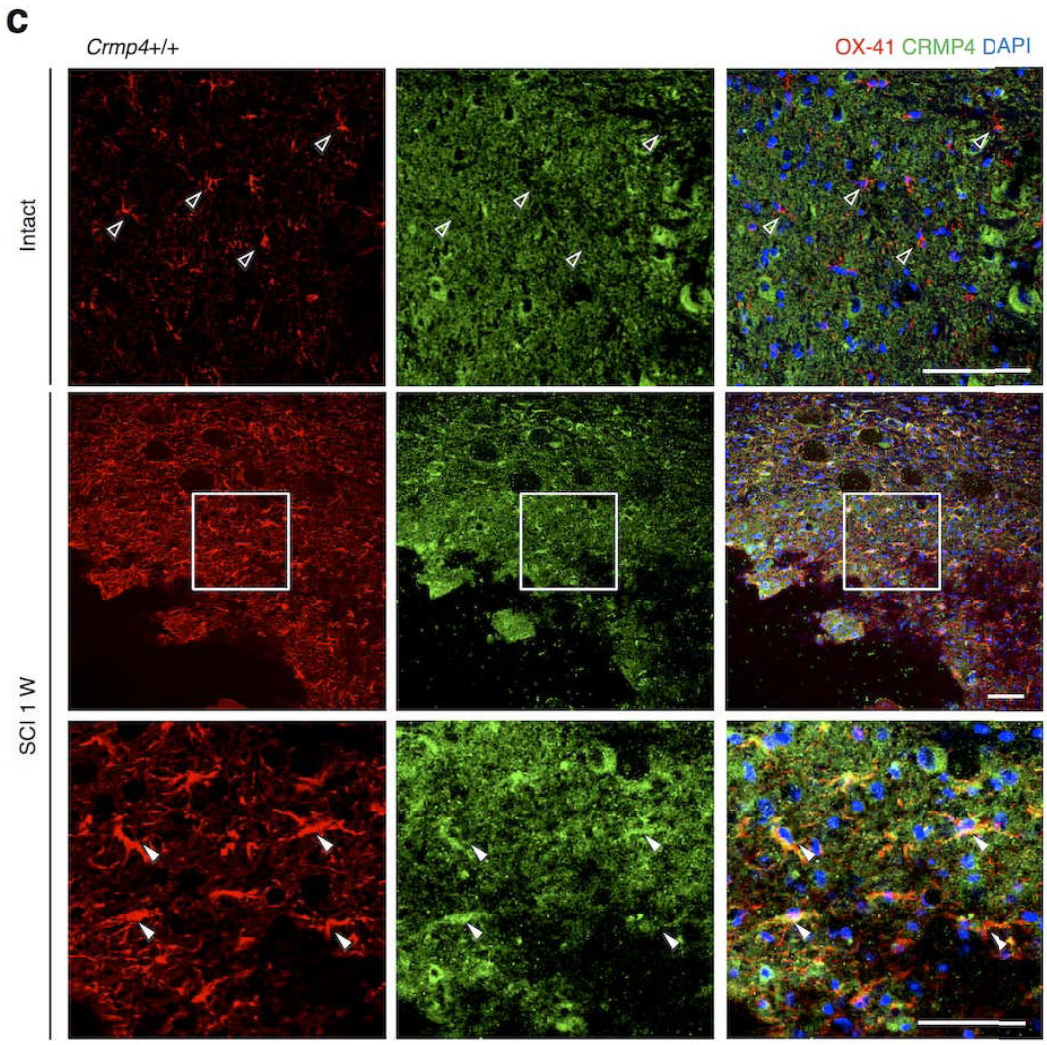

Figure 3.2.2

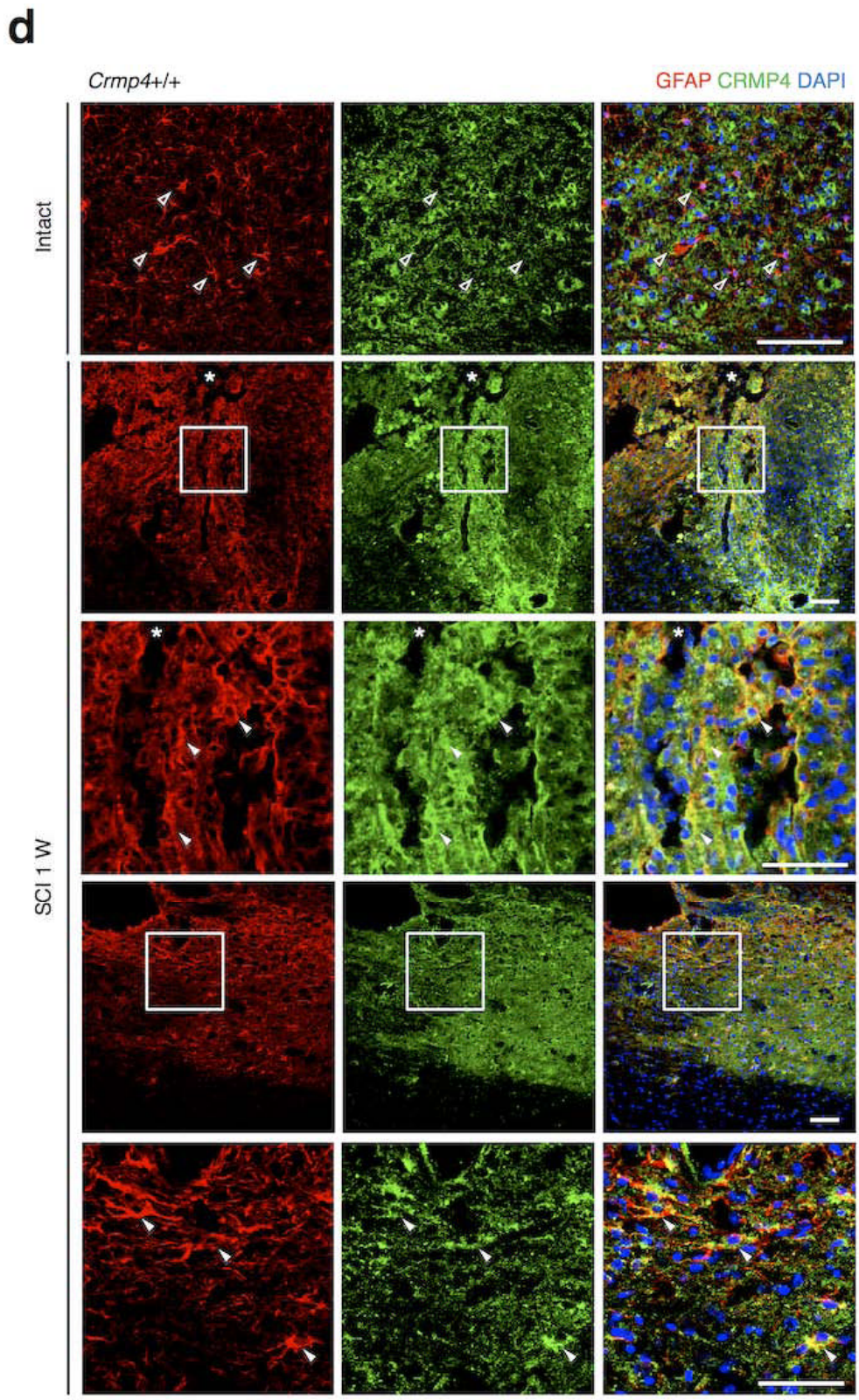

Figure 3.2.2

Figure 3.2.2 Expression changes of CRMP4 in spinal motoneurons and glial cells after SCI. Immunohistochemical analysis of the expression of CRMP4 of the intact and injured spinal cords 1 week after transection (SCI 1 W). (**a**) Representative images from cross sections of spinal cord show double immunofluorescent staining of Nissl (the marker for neurons; red) and CRMP4 (green). CRMP4 staining was apparent in Nissl-positive motoneurons in the ventral horn (solid arrowheads) both in intact and injured spinal cords from control *Crmp4*+/+ mice. This CRMP4 signal was undetectable in the intact *Crmp4*–/– spinal cord. (**b**) Co-localization of CRMP4 (green) and MAP2 (red) immunopositive structures, which labeled neuronal cell bodies and dendrites, both in the ventral horn of intact and transected spinal cords. (**c-d**) Immunohistochemical analysis of the expression of CRMP4 in microglia/macrophage and astrocytes. Images of sagittal sections show double immunofluorescent staining for CRMP4 (green) and OX-41 (red), the marker for microglia/macrophage (**c**), or GFAP, a marker for normal and reactive astrocytes (**d**). In the intact spinal cord, the red signals in the resting OX-41-positive microglia/macrophage and GFAP-positive astrocytes did not co-localize with the green signals of CRMP4 (open arrowheads). However, 1 week after SCI, CRMP4 signals were evident in these activated cells (arrowheads) adjacent to lesion epicenter and astroglial scar. Nuclei were counterstained with DAPI (blue) in the same view in each section. Asterisks in d indicate the lesion site. W, weeks. Scale bars: 100 μm. (Nagai et al., 2015)

Suppressed microtubule destabilization of axons in injured *Crmp4*–/– spinal cords

Given the increased expression of inhibitory and toxic forms of CRMP4 after SCI, I next analyzed the effect of loss of function of CRMP4 on microtubule polymerization in injured axons in the acute phase of SCI. A previous study has shown that polymerized microtubule levels in white matter axons were decreased at 2 h post SCI[19]. I conducted immunostaining with anti-Glu-tubulin antibody to measure the polymerized forms of microtubules after SCI. In intact spinal cord, Glu-tubulin was present in a line along the Tuj1-positive axons in the white matter both in control *Crmp4*+/+ and in *Crmp4*–/– mice (**Fig. 3.2.3a**). To examine the microtubule stability in Tuj1-positive axons in the dorsal white matter of spinal cord after lesion, I measured the ratio of Glu-tubulin-positive axon (stable axon: white in **Fig. 3.2a,b**) to full-length axon (purple in **Fig. 3.2a,b**). At 2 h post SCI, control mice showed a 67.5±3.08% reduction in the relative length of Glu-tubulin-positive axons in the dorsal white matter about 3 mm rostral to the injury site **(Fig. 3.2.3b**). However, this decrease of microtubule polymerization in injured axons was reduced to 48.6±3.09% in *Crmp4*–/– mice (**Fig. 3.2.3b**, arrowheads; $P < 0.05$ compared with **Fig. 3.2.3c**, SCI 2-h control). This result

indicates that deletion of CRMP4 contributes to stabilizing microtubules in the acute phase of SCI.

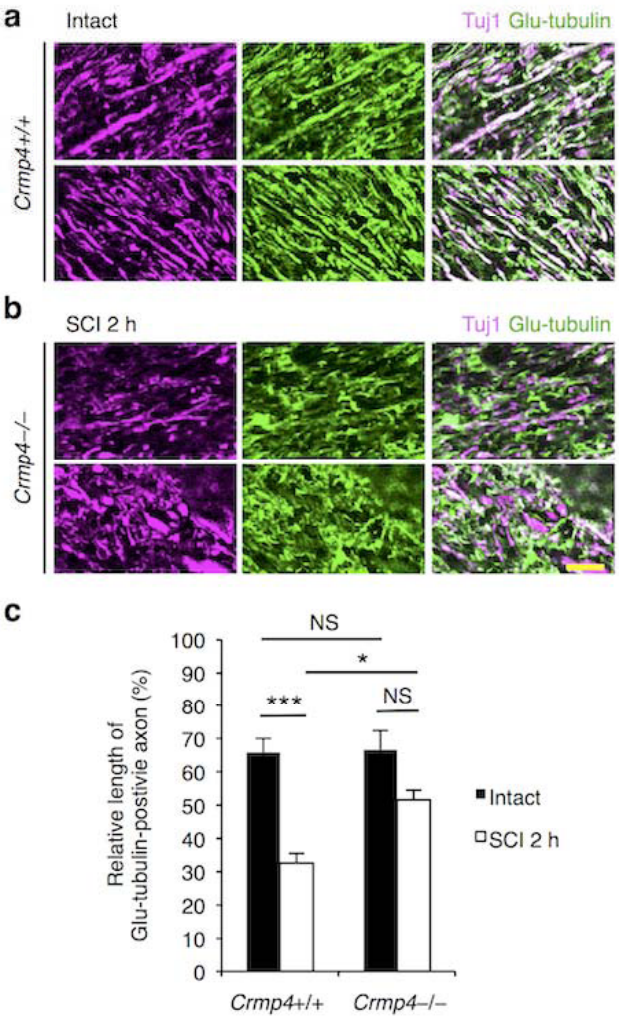
a
Intact
Tuj1 Glu-tubulin
Crmp4+/+
b
SCI 2 h
Tuj1 Glu-tubulin
Crmp4−/−
c
NS
*
***
NS
Relative length of Glu-tubulin-postivie axon (%)
100
90
80
70
60
50
40
30
20
10
0
Intact
SCI 2 h
Crmp4+/+
Crmp4−/−

Figure 3.2.3

Figure 3.2.3 Suppression of microtubule depolymerization in the axons of the injured spinal cord on deletion of CRMP4. (**a**,**b**) Representative images of double immunohistochemistry for neuron-specific class III β-tubulin, Tuj1 (purple) and Glu-tubulin (green), which is abundant in polymerized microtubules. Glu-tubulin-positive stable microtubules showed a distribution along the Tuj1-positive axons in the white matter of intact spinal cords (**a**; white). This distribution was remarkably reduced at 2 hours after SCI (SCI 2 h) in *Crmp4*+/+ mice in the dorsal white matter (**b**). However, the staining pattern of Glu-tubulin was significantly preserved in *Crmp4*−/− mice (**b**; white). Scale bar: 20 μm. (**c**) Quantification of relative length of Glu-tubulin-positive microtubules to Tuj1-positive axons in the dorsal white matter within 3 mm rostral and caudal to the lesion epicenter. n = 6 mice for each genotypes. *, $P < 0.05$, ***, $P < 0.001$. Statistical analysis was performed using two-way ANOVA followed by Tukey's test. Data are mean ± S.E.M. h, hours; NS, no significant difference. (Nagai et al., 2015)

CRMP4 in glial cells contributes to inflammatory response and scarring

To clarify the role of CRMP4 upregulation in activated microglia/macrophage and reactive astrocytes (**Fig. 3.2.2c,d**), I next assessed the degree of inflammation in *Crmp4*−/− mice after traumatic injury, which induces secondary tissue damage and scarring[31].

First, I utilized a non-traumatic inflammation model to clarify the role of CRMP4 in the inflammatory response. Microinjections of Zymosan A into lateral white matter of thoracic spinal cord caused marked activation of Iba1-positive microglia/macrophages and GFAP-positive astrocytes at 3 days post injection in control mice (**Fig. 3.2.4a**). These activations were undetectable around PBS injection sites, indicating that the effect of micropipette insertion was negligible. In contrast, *Crmp4*−/− exhibited dramatic reduction in the area of inflammatory activation over the Zymosan A-injection site ($P < 0.05$ compared with control mice, **Fig. 3.2.4a-c**). Additionally, the protein expression level of Tumor necrosis factor α (TNFα) was elevated in Zymosan A-injected spinal cord of control mice when compared with PBS-injected control mice (167±20.6%, $P < 0.05$, **Fig. 3.2.4d,e**). The TNFα level after Zymosan A injection was

significantly reduced by deletion of CRMP4 (34.8±22.6%, $P < 0.05$, compared with Zymosan A-injected control mice, **Fig. 3.2.4d,e**). As TNFα is a pro-inflammatory cytokine secreted by microglia/macrophages and reactive astrocytes, this result indicated the reduction in non-traumatic inflammation upon CRMP4 deletion.

I next examined inflammatory responses in the spinal cord after SCI. Microglia/macrophage and astrocytes exhibit small, compact somata bearing many long, thin, ramified processes at their resting state. However, activated microglia/macrophage and reactive astrocytes demonstrate marked cellular hypertrophy and retraction of cytoplasmic processes[92,93]. At 1 week post SCI, microglia in the dorsal horn of control spinal cords at 1.5 mm caudal to lesion epicenter exhibited the activated phenotype (**Fig. 3.2.5a**). In contrast, *Crmp4*−/− mice showed moderate expression of resident microglia exhibiting the quiescent or resting type morphology in both white and gray matters of spinal cord (**Fig. 3.2.5b**). Numbers of Iba1-positive cells and activated Iba1-positive cells, which are determined with processes shorter than the diameters of cell bodies[92], in dorsal horn of *Crmp4*−/− spinal cord were decreased 13.7±1.86% and 72.1±3.69%, respectively, when compared to control spinal cord (**Fig. 3.2.5g**, $P < 0.05$; **Fig. 4h**, $P <$

0.001). GFAP-positive astroglia demonstrating swollen hypertrophic appearance were distributed in both white and gray matters in injured control spinal cords (**Fig. 3.2.5c**). Although CRMP4 deletion had no effect on levels of such astroglial morphology in the dorsal horn of injured spinal cord (**Fig. 3.2.5d**), *Crmp4*−/− spinal cord exhibited 23.6± 2.06% reduction in immunoreactivity of GFAP in the dorsal horn when compared with control spinal cord (**Fig. 3.2.5i**, $P < 0.05$). These results indicate that the activation of microglia/macrophage and astrocytes after injury observed in *Crmp4*+/+ mice was minimal in *Crmp4*−/− mice.

Third, I assessed scar formation after SCI in *Crmp4*−/− mice. The lesion scar in traumatic SCI consists of a fibrous scar at the lesion core surrounded by a glial scar[2]. I observed a collagen IV-positive fibrous scar around the lesion epicenter in control spinal cord at 1 week post SCI (**Fig. 3.2.5e**). However, in *Crmp4*−/− spinal cords, an 85.4±11.9% reduction in collagen IV-positive scar was observed (**Fig. 3.2.5f,j**, $P <$ 0.05 compared with control mice,). These findings indicate that CRMP4 deletion prevents scarring by moderating inflammatory responses after SCI.

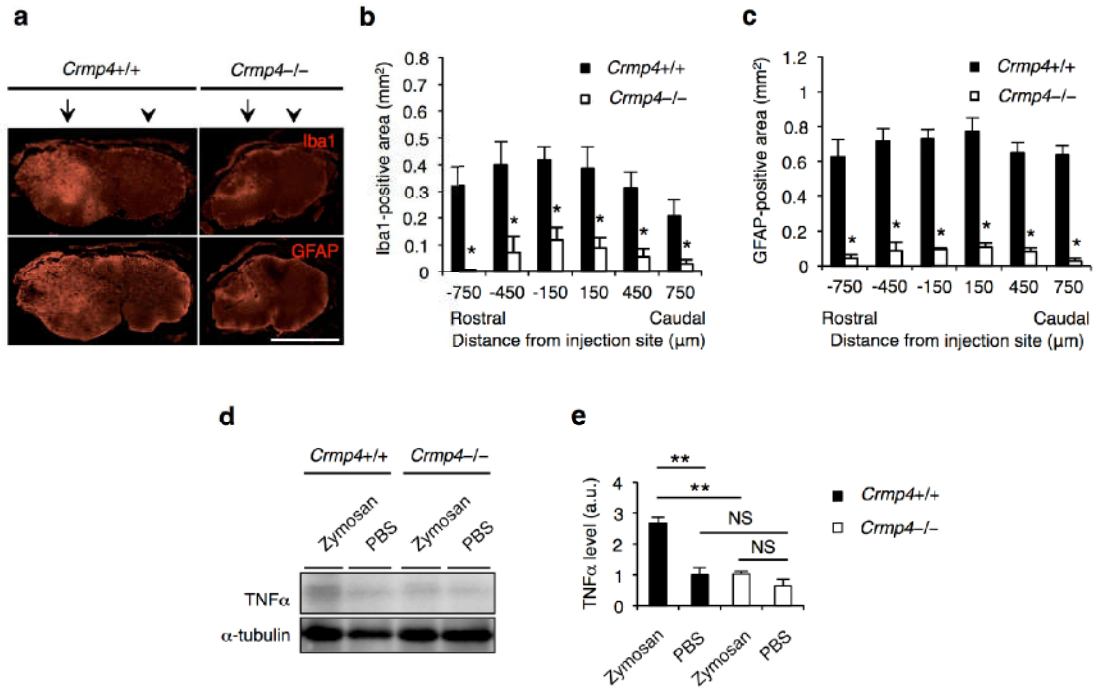

Figure 3.2.4 CRMP4 deletion reduces non-traumatic inflammation. (**a**) Representative transverse images of thoracic spinal cords 150 μm rostral to the injection site stained with anti-Iba1 (marker for microglia/macrophages) and anti-GFAP (marker for astrocytes*)* antibodies at 3 days post induction of non-traumatic inflammation by Zymosan A. Arrows, Zymosan A injection site; arrowheads, PBS injection site. Intraspinal micropipette insertion was confirmed to be non-traumatic by failure of PBS microinjection to activate microglia and astroglia. Scale bars = 1000 μm. (**b, c**) Areas of quantified microglial and astroglial activation in transverse sections taken every 300 μm around the injection site. n = 3 mice. *, $P < 0.05$ compared with *Crmp4*+/+ controls. Statistical analysis by unpaired Student's *t* test. (**d, e**) Western blotting analysis with anti-Tumor necrosis factor alpha antibody after Zymosan A- or buffer-injection to spinal cords (n = 3 animals). **, $P < 0.01$. Statistical analysis was performed using two-way ANOVA followed by Tukey's test. Data are mean ± S.E.M. PBS, phosphate-buffered saline; TNFα, Tumor necrosis factor alpha; NS, no significant difference. (Nagai et al., 2015)

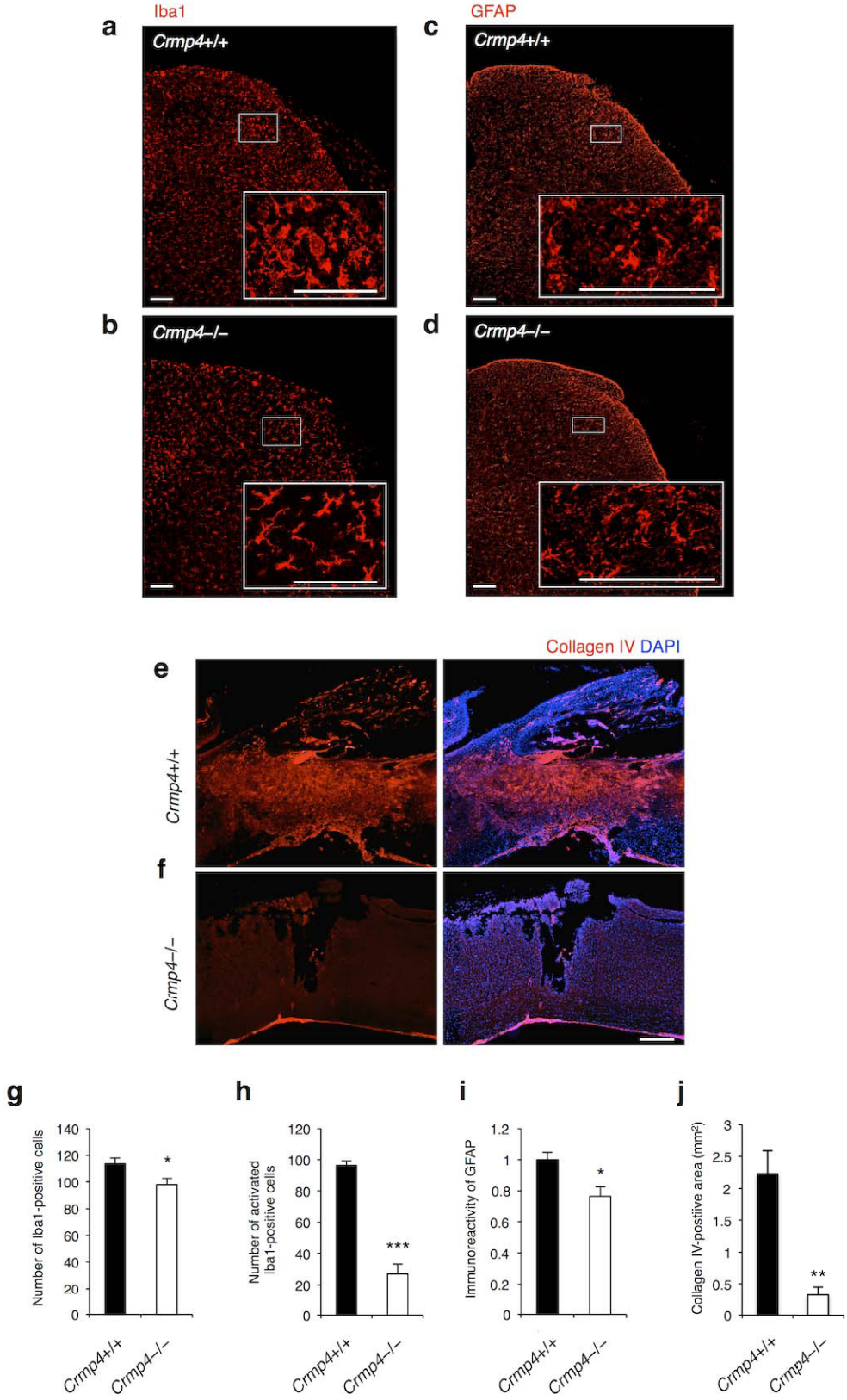
a
Iba1
Crmp4+/+
b
Crmp4–/–
c
GFAP
Crmp4+/+
d
Crmp4–/–
e
Collagen IV DAPI
Crmp4+/+
f
Crmp4–/–
g
Number of Iba1-positive cells
140
120
100
80
60
40
20
0
*
Crmp4+/+
Crmp4–/–
h
Number of activated Iba1-positive cells
120
100
80
60
40
20
0
***
Crmp4+/+
Crmp4–/–
i
Immunoreactivity of GFAP
1.2
1
0.8
0.6
0.4
0.2
0
*
Crmp4+/+
Crmp4–/–
j
Collagen IV-positive area (mm²)
3
2.5
2
1.5
1
0.5
0
**
Crmp4+/+
Crmp4–/–

Figure 3.2.5

Figure 3.2.5 Deletion of CRMP4 suppresses inflammatory responses and scar formation after SCI. (**a,b**) Representative images of immunohistochemistry for Iba1, a marker for microglia/macrophage, at 1.5 mm caudal to tissue lesions at 1 week after SCI. While *Crmp4*+/+ mice with SCI demonstrated activated forms, determined with longer processes than the soma diameter, *Crmp4*–/– mice exhibited resting morphology of microglia/macrophage. (**c,d**) GFAP staining revealed hypertrophic phenotype of reactive astrocytes in dorsal horn of injured spinal cords. Although no clear difference between *Crmp4*+/+ and *Crmp4*–/– spinal cords in terms of morphological changes in astrocytes was observed, there seemed to be decreased immunoreactivity of GFAP signals in injured *Crmp4*–/– spinal cords compared with controls. (**e,f**) Representative images of sagittal sections of collagen IV-positive scar formation at 1 week after SCI. (**g-i**) Quantifications of inflammatory responses in the dorsal horn at 1.5 mm caudal to injury site. *Crmp4*–/– mice exhibited decreased total number of Iba1-positive cells (**g**), reduced number of activated Iba1-positive cells (**h**) and suppressed immunoreactivity of GFAP (**i**) when compared with control mice (n = 5 mice for each genotypes). (**j**) Quantitative analysis of the area of collagen IV-positive scar tissue shows dramatic reduction of scarring in *Crmp4*–/– spinal cords compared with *Crmp4*+/+ one (n = 5 mice for each genotypes). *, $P < 0.05$, **, $P < 0.01$, ***, $P < 0.001$ compared with *Crmp4*+/+ controls. Statistical analysis was performed using an unpaired Student's *t* test. Data are mean ± S.E.M. Scale bars: 100 μm in **a**-**d**, 500 μm in **e**,**f**. (Nagai et al., 2015)

Neuroprotection at the lesion site in transected *Crmp4*–/– spinal cord

Extensive inflammation-induced tissue injury causes impaired CNS function because of delayed secondary neuronal damage, such as neuronal loss and demyelination[94,95]. Additionally, it has been suggested that the calpain-mediated C-terminus truncation product of CRMP4 (tCRMP4) is associated with neuronal apoptosis after neurotoxin treatment[78]. To analyze the effect of CRMP4 deletion on cell survival in lesioned spinal cords, I performed the TUNEL assay (terminal deoxynucleotidyl transferase (TdT)-mediated deoxyuridine triphosphate-biotin nick end labeling) to detect apoptosis in both groups at 1 week post injury, a time point corresponding to the peak of secondary apoptosis at the lesion site[96]. *Crmp4*–/– mice showed 70.2±2.25%, 68.2±3.52%, 72.8±7.44% and 64.4±3.12% reductions in the number of TUNEL-positive apoptotic cells at 1 mm rostral to, 1 and 2 mm caudal to, and central to the lesion epicenter, respectively ($P < 0.05$ compared with control mice, **Fig. 3.2.6a,b**). Next, to examine the effect of CRMP4 deletion on tissue loss after SCI, I performed Nissl and myelin staining in serial cross sections over the lesion epicenter at 1 and 4 weeks post transection. The *Crmp4*–/– spinal cord exhibited spinal tissue sparing at lesion epicenter

and increased neuronal cell survival at caudal side to injury site (**Fig. 3.2.6c**). Myelin staining revealed that CRMP4 deletion spared white matter area at core and caudal to lesion, indicating reduced demyelination when compared with control spinal cords at 4 weeks post SCI (**Fig. 3.2.6d**). The differences in spinal tissue volume were not observed between *Crmp4*$^{-/-}$ spinal cord and control one at 1 week post SCI (**Fig. 3.2.7a, 3.2.8a**), suggesting that tissue sparing at 4 weeks post injury was not due to variance of lesion but to neuroprotection against SCI with CRMP4 suppression (**Fig. 3.2.7b, 3.2.8b**). These results suggest that CRMP4 deletion has a neuroprotective effect on cells at the lesion site after SCI, thereby creating a permissive environment for the regrowth of axons in the injured spinal cord.

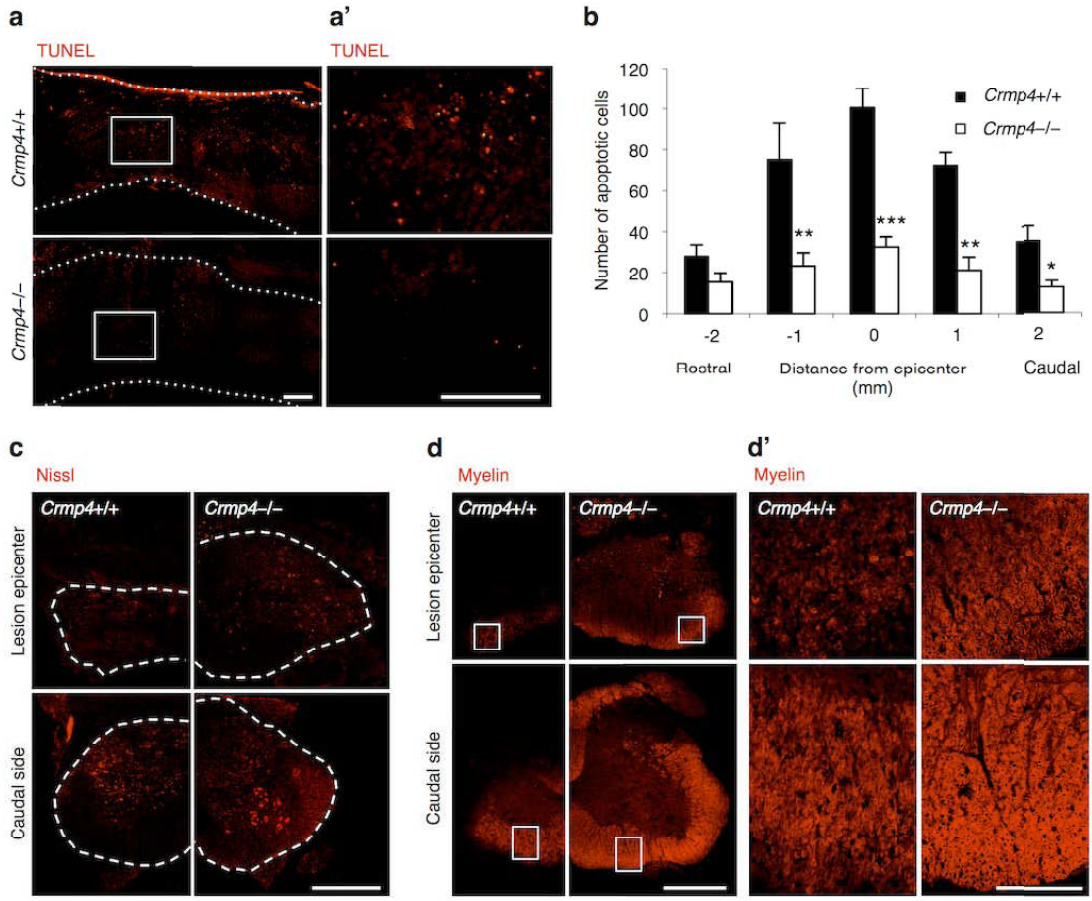

Figure 3.2.6 Decreased apoptotic cell death and demyelination in the injured spinal cord of *Crmp4–/–* mice. (**a**) Representative images of sagittal sections of TUNEL-positive apoptotic cells at 1 week post SCI. (**a'**) Magnified images of the indicated areas in **a**. (**b**) Quantitative analysis of the numbers of TUNEL-positive apoptotic cells showed decreased apoptotic cells in *Crmp4–/–* spinal cords when compared with those in *Crmp4*+/+ controls (*, $P < 0.05$, **, $P < 0.01$, ***, $P < 0.001$). Statistical analysis was performed using an unpaired Student's *t* test. n = 5 mice for each genotypes. Data are mean ± S.E.M. (**c**) Nissl staining in cross sections of the center and 1.5 mm caudal to the injury site revealed increased cell survival in *Crmp4–/–* spinal cords when compared with in *Crmp4*+/+ controls at 4 weeks post SCI. (**d**) Images from cross sections of center and 900 μm caudal to injury site with myelin staining. *Crmp4–/–* spinal cords showed higher density of myelin signals and larger area of white matter at both positions when compared with in *Crmp4*+/+ controls at 4 weeks post SCI. Scale bar: 100 μm in **a,a',d'**, 500 μm in **c,d**. (Nagai et al., 2015)

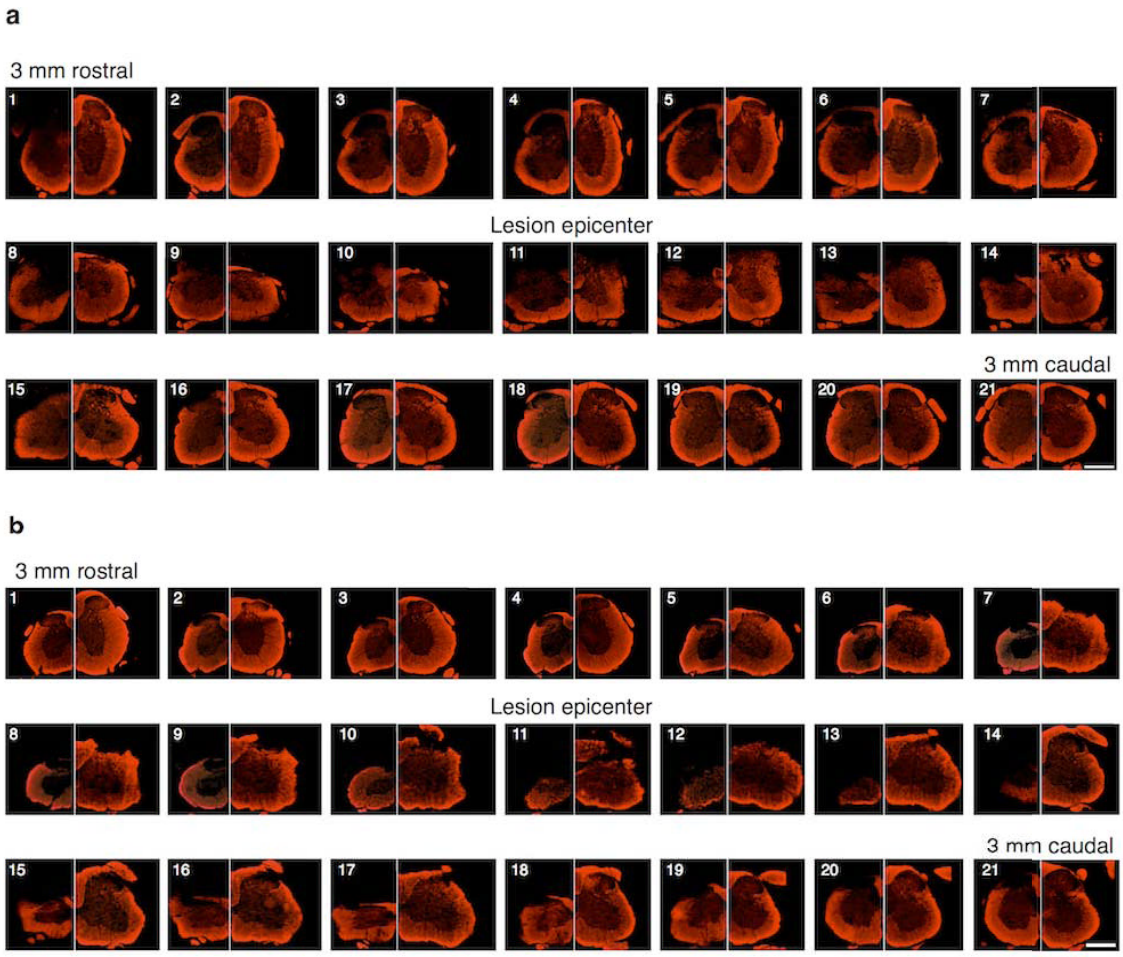

Figure 3.2.7 Serial cross sections from *Crmp4*+/+ and *Crmp4*–/– mice after SCI with myelin staining. Myelin staining of serial cross sections taken every 300 μm reveals demyelination over the lesion epicenter (#11). Sections #1–10 are rostral and #12–21 are caudal to the injury site. The left half of each spinal cord section illustrated is from a *Crmp4*+/+ mouse and the right half is from a *Crmp4*–/– mouse. The areas of myelin-positive white matter are not different among samples at 1 week post SCI, indicating that the dorsal transections to the animals were of uniform extent (**a**). However, at 4 weeks post injury, *Crmp4*–/– spinal cord exhibits significantly increased sparing of tissue, including white matter, when compared with control (**b**). The images of #11 and #14 in **b** are shown in **Fig. 3.2.6d**. Scale bar: 500 μm. (Nagai et al., 2015)

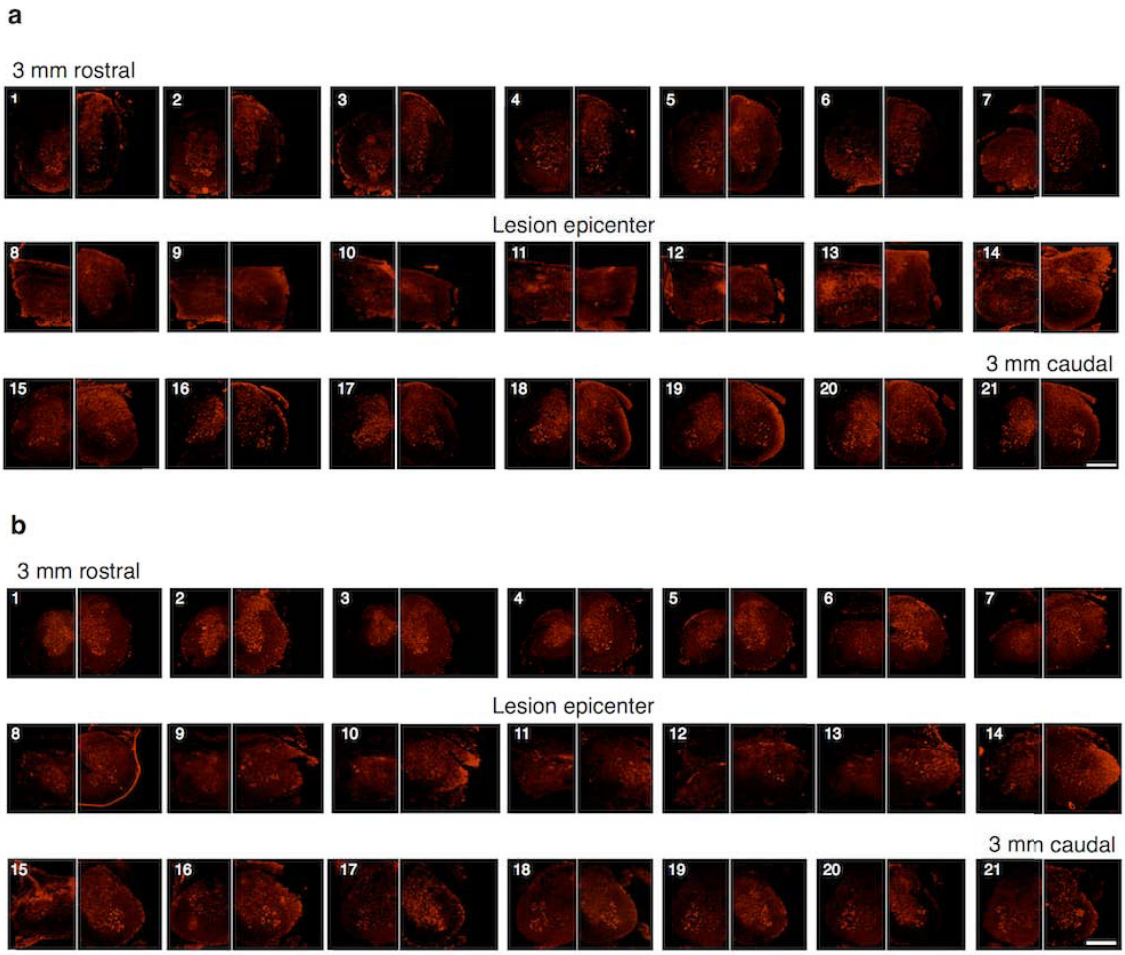

Figure 3.2.8 Serial cross sections from *Crmp4*+/+ and *Crmp4*–/– mice after SCI with Nissl staining. Nissl staining of serial cross sections taken every 300 μm reveals demyelination through the lesion epicenter (#11). Sections #1–10 are rostral and #12–21 are caudal to the injury site. The left halves of the spinal cord sections are from a *Crmp4*+/+ mouse and the right halves are from a *Crmp4*–/– mouse at 1 week post injury (**a**) or at 4 weeks post injury (**b**). The images of #11 and #16 in **b** are shown in **Fig. 3.2.6c**. Scale bar: 500 μm. (Nagai et al., 2015)

Deletion of CRMP4 enhances axonal growth in injured spinal cord

To further characterize the role of CRMP4 in limiting axonal growth *in vivo,* I performed immunohistochemical analyses of spinal cords after injury, avoiding the sections of the control spinal cords that had large cavitations, to obtain a clearer histological comparison with sections of *Crmp4*−/− spinal cords. I detected an increased density of growth-associated protein 43 (GAP43)-positive regenerating or sprouting axons caudal to the lesion site in *Crmp4*−/− mice at 18 days post SCI, while almost no expression of GAP43 in axons within and caudal to the injury site was observed in control mice (**Fig. 3.2.9a**). To examine which types of spinal fibers are GAP43-positive, I conducted immunostaining of GAP43 in cross sections caudal to the injury site (**Fig. 3.2.9b**). In control mice, GAP43-positive fibers were observed only in the dorsal horn (arrowheads), which are ascending tracts from dorsal root ganglion. In contrast, *Crmp4*−/− spinal cords exhibited clear signals of GAP43 at the location of descending CST fibers (arrows) as well as ascending tracts in the dorsal horn (arrowheads). To confirm the elevated axonal growth, I also performed immunoblotting analysis with anti-GAP43 antibody using tissue samples from intact and injured spinal cords of both

groups. I detected GAP43 protein expression in the spinal cords from control and *Crmp4*–/– mice at 18 days post SCI, but not in the intact spinal cords. I observed a significantly higher level of GAP43 protein in *Crmp4*–/– spinal tissue than in controls (**Fig. 3.2.9c,d**).

In this study, I utilized a 1.5-mm-depth near-complete dorsal transection model[97] to sever the whole gray matter of the spinal cord and a group of defined pathways, including raphespinal and corticospinal tract (CST) axons and all their branches, leading to hindlimb paralysis. The serotonergic (5-hydroxytryptamine [5-HT]-positive) raphespinal system contributes to locomotor circuitry and can be assessed in an anterograde fashion by simple immunohistology, since it is the only source of serotonergic input to the adult spinal cord. In control mice with dorsally transected spinal cords, 5-HT-immunoreactive fibers were observed as a few subsets caudal to the lesion site at 4 weeks post SCI (**Fig. 3.2.10a**). However, in *Crmp4*–/– transected spinal tissue, a high density of 5-HT-positive fibers was detectable in parasagittal sections on the far side of the lesion (caudal to the epicenter). *Crmp4*–/– spinal cord exhibited 173 ±30.1% increase in immunoreactivity of 5-HT within 1-2 mm caudal to the injury site

when compared to controls (**Fig. 3.2.10e**, $P < 0.05$). Cross sections of spinal cord at a level 4 mm caudal to a near-complete transection were also examined for 5-HT-positive profiles (**Fig. 3.2,10b**). As previously reported[23], the highest density of innervations was observed in the ventral horn in both groups rostral to the lesion site. 5-HT fiber density at 3 mm rostral to the lesion was not different between genotypes (**Fig. 3.2.10b**). Although the immunoreactivity of serotonergic fibers at the 4-mm-caudal level was essentially undetectable in injured control spinal cord, a significant proportion of raphespinal fibers were observed in the ventral horn of the distal cord following injury in *Crmp4*−/− mice (**Fig. 3.2.10b**).

To examine whether deletion of CRMP4 induces CST growth, I used a yellow fluorescent protein (YFP)-expressing mouse line (YFP-H)[81]. In this transgenic mouse, corticospinal neurons in layer V of the cerebral cortex and their projecting axons in the spinal cord are strongly YFP-positive, with relatively weak YFP signals in some ascending dorsal column axons from dorsal root ganglion neurons, projections in the lateral and ventral columns, and motoneurons[81]. Because of its strong YFP signal in CST, this mouse line was used for evaluation of recovery from SCI[98]. Proximal to the

lesion at 4 weeks post SCI, the main CST appears as a tight bundle of fibers, with the labeled fibers neither entering nor growing beyond the lesion site in sagittal sections from control mice (**Fig. 3.2.10c**; solid arrowheads). To summarize the pattern of CST fiber growth rostral and caudal to the injury, I reconstructed CST fibers by overlaying all the serial microscopic images from parasagittal sections that included YFP-positive CST fibers (**Fig. 3.2.10c'**). As YFP expressions are controlled by the neuron-specific *Thy1* promotor elements, the YFP signals were not restricted in corticospinal neurons. To obtain clear structure of dCST axons, I cropped dCST and put together with GFAP-positive glial scar of the same sections (**Fig. 3.2.10c''**). The control mice exhibited almost no fibers in normal CST locations 3 mm caudal to the lesion site (**Fig. 3.2.10d**; open arrowheads). In contrast, significant numbers of YFP-positive fibers growing into the lesion scar and through cysts were observed in the injured *Crmp4*−/− spinal cord (**Fig. 3.2.10c**; solid arrow, **3.2.10c',c''**). Moreover, I observed a higher density of YFP-positive CST axons presenting in their normal position at 3 mm caudal to the lesion in *Crmp4*−/− mice when compared to the control mice (**Fig. 3.2.10d**; solid arrow, **Fig. 3.2.10f**, $P < 0.05$). Taken together, the evidence shows that the deletion of

CRMP4 enhanced axonal regrowth or sprouting after near-complete spinal transection.

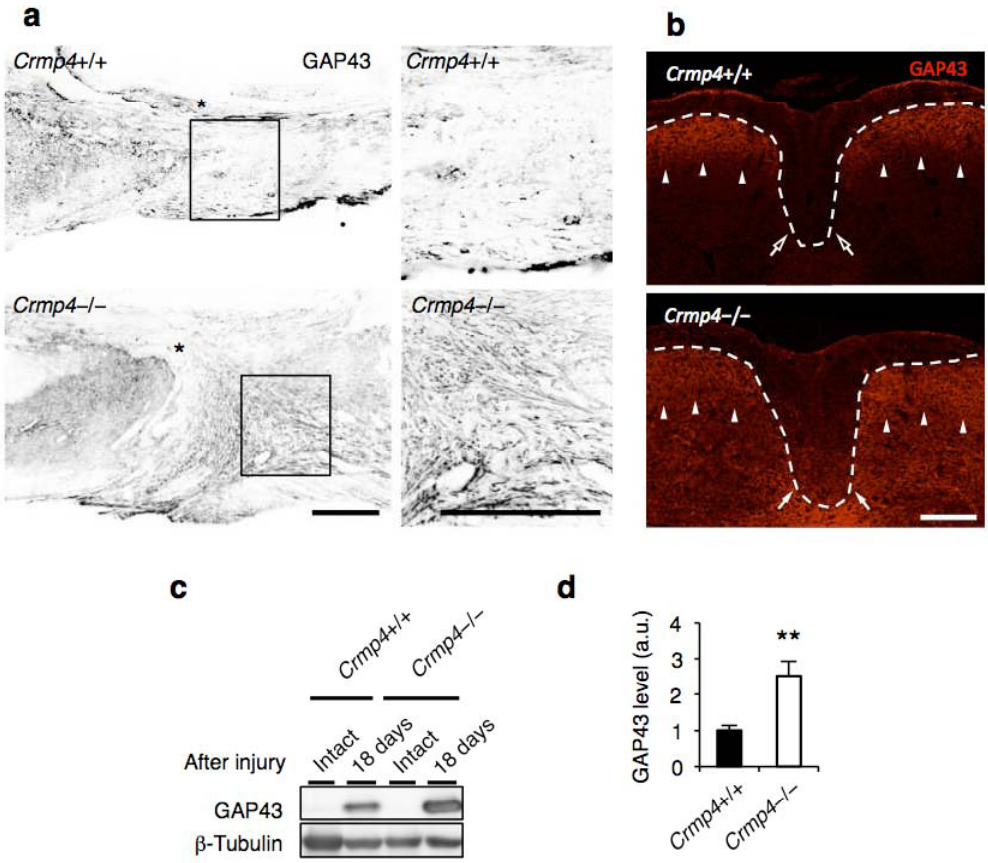

Figure 3.2.9 Enhanced axonal growth in *Crmp4*–/– mice after near-complete transection. (**a**) Representative sagittal sections of immunohistochemical analysis of GAP43-positive axons at 18 days after SCI. GAP43-positive straight growing axons were evident in *Crmp4*–/– mice, but not in controls. (**b**) Axonal growth in cross sections at 1.5 mm caudal to the lesion site at 4 weeks after injury was detected by immunostaining with anti-GAP43 antibody. Ascending fibers from dorsal root ganglia were GAP43-positive in both genotypes (arrowheads). Although GAP43-positive fibers were not detected at the location of descending CST in a *Crmp4*+/+ spinal cord (open arrows), CRMP4 deletion promotes GAP43-positive fiber growth at the dCST location (arrows) and within lateral horn, possibly suggesting growth of CST axonal arbors. (**c,d**) Western blotting analysis with anti-GAP43 antibody (n = 6 mice for each genotype). Statistical analysis was performed using an unpaired Student's *t* test. Data are mean ± S.E.M. Scale bars: 300 μm in **a**, 100 μm in **b**. d, days. (Nagai et al., 2015)

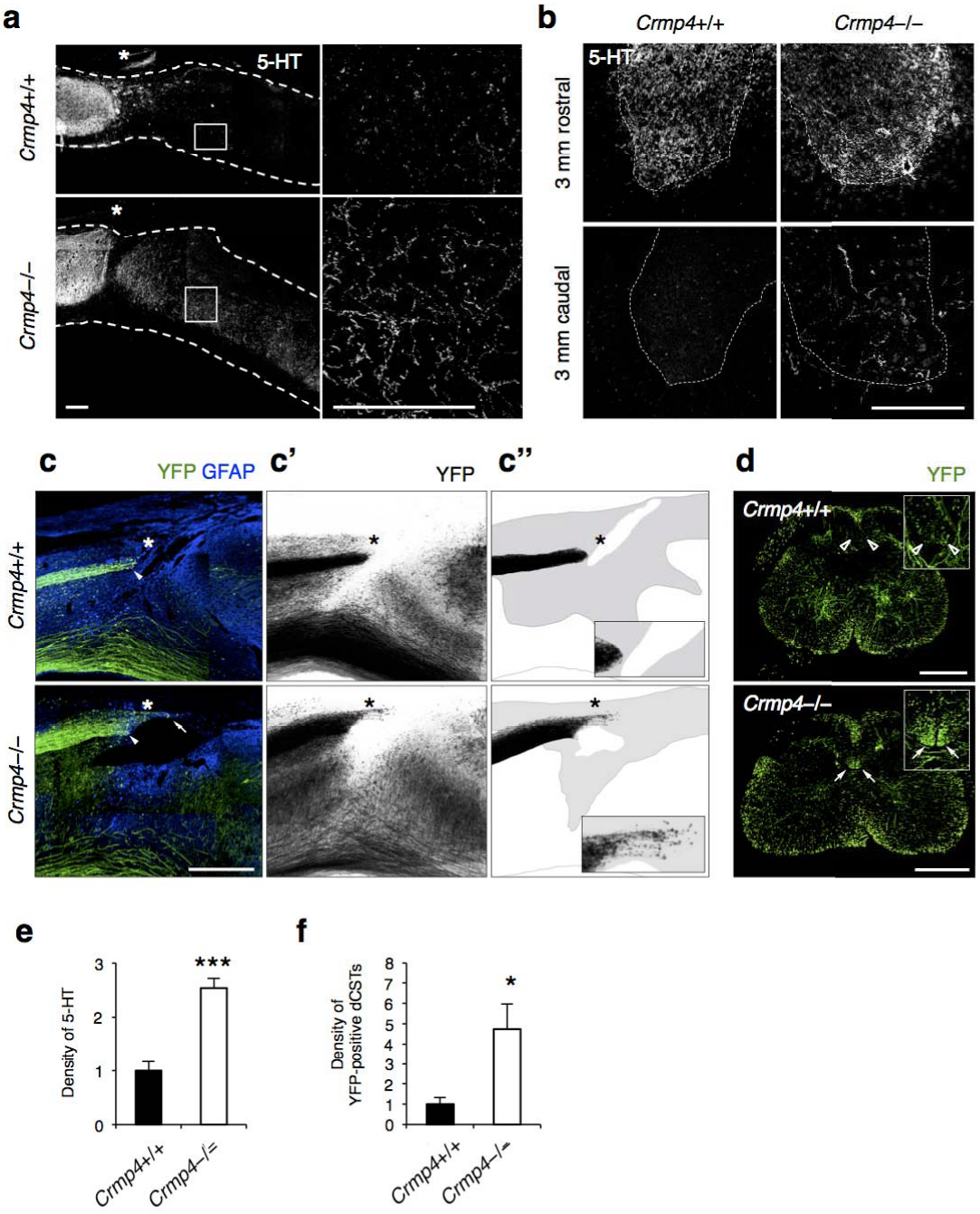
a
5-HT
Crmp4+/+
Crmp4–/–
b
Crmp4+/+
Crmp4–/–
5-HT
3 mm rostral
3 mm caudal
c
YFP GFAP
c'
YFP
c''
d
YFP
Crmp4+/+
Crmp4–/–
e
Density of 5-HT
***
Crmp4+/+
Crmp4–/–
f
Density of YFP-positive dCSTs
*
Crmp4+/+
Crmp4–/–

Figure 3.2.10

Figure 3.2.10 Enhanced axonal growth of raphespinal and coticospinal tracts in *Crmp4*–/– mice after near-complete transection.

(**a**) Images from sagittal sections of 5-HT immunohistochemical analysis revealed 5-HT-positive rectilinear profiles of raphespinal tract axons caudal to the lesion site in *Crmp4*–/– mice at 4 weeks after SCI, while 5-HT signals were not apparent in controls. (**b**) Representative cross sections of spinal cords stained with anti-5-HT antibody at levels 4 mm rostral or caudal to the injury site at 4 weeks after SCI. (**c**) Near-complete dorsal transection of spinal cord transects the main descending CST projection (solid arrowheads) at 4 weeks after SCI. Reconstructed (**c'**) and camera lucida drawings (**c''**) of YFP-labeled CST axons in all consecutive parasagittal sections. Gray areas in g'' indicate the GFAP-positive glial scar tissues developing at the lesion site. The core and caudal side to the lesion epicenter (asterisks) were devoid of YFP-labeled CST in *Crmp4*+/+ mice. In contrast, YFP-labeled fibers were significantly apparent at the injury site along cavitation in *Crmp4*–/– mice (**c**; solid arrows). (**d**) Representative images of cross sections of 3 mm caudal to the lesion site at 4 weeks after transection (**d**). While the absence of YFP-positive CST (open arrowheads) were observed in the control mice, injured *Crmp4*–/– spinal cords showed a greater number of CST axons at the CST location (solid arrows in **d**). (**e**) Quantitative analysis of immunoreactivity of 5-HT within 1-2 mm caudal to the lesion site in parasagittal sections (n = 5 mice for each genotype). (**f**) Quantification of immunoreactivity of YFP-positive dCST fibers at the location (n = 4 mice for each genotype). Asterisks in the images of sagittal sections indicate the lesion epicenters. The left side is rostral in all the images of parasagittal sections. *, $P < 0.05$, **, $P < 0.01$, ***, $P < 0.001$ compared with *Crmp4*+/+ controls. Statistical analysis was performed using an unpaired Student's *t* test. Data are mean ± S.E.M. Scale bars: 300 μm in **a,b**, 500 μm in **c,d**. (Nagai et al., 2015)

Locomotor recovery in *Crmp4*–/– mice after SCI

To examine the behavioral function in *Crmp4*–/– mice after SCI, I used the Basso Mouse Scale for locomotion (BMS)[86] to assess the hindlimb motor function. In all the mice used in this study, hindlimb movement was completely normal (BMS score: 9) before injury and abolished (BMS score: 0-1) immediately after near-complete transection. At 4 weeks post SCI, hindlimb showed slight recovery from paralysis in control mice (average BMS score: 1.6 ± 0.3, n = 7, mean ± S.E.M., **Fig. 3.2.11a,b**), in agreement with results from a previous study using a near-complete-transection model in wild-type mice[97]. In contrast, the *Crmp4*–/– mice had significantly higher BMS scores (5.3 ± 0.3, mean ± S.E.M., n = 7, **Fig. 3.2.11a,c**). Notably, many of these mice could move all joints of the hindlimbs freely and could support their own weight around 1 week post SCI, which is considered early for the recovery phase of an injury (**Fig. 3.2.11a,d**).

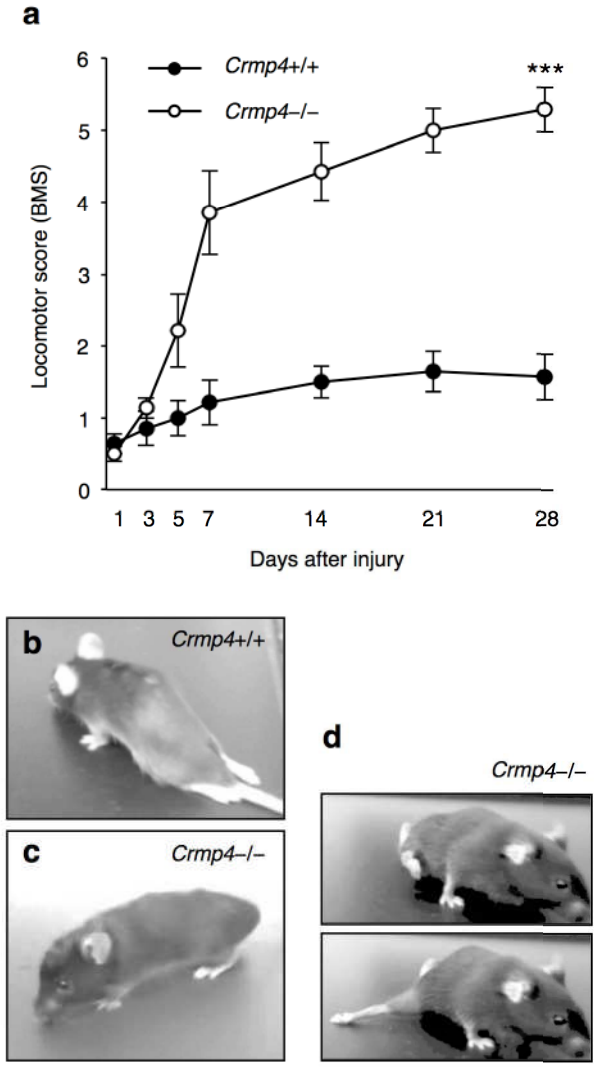

□

Figure 3.2.11 Improvement of locomotion after SCI in mice lacking CRMP4. (**a**) Functional analysis of open field locomotor activity by BMS scoring up to 28 days after near-complete transection of spinal cord in *Crmp4*+/+ and *Crmp4*–/– mice. Note that locomotor recovery in *Crmp4*–/– mice was significant from early stages post-SCI (n = 7 mice for each genotype). ***, $P < 0.001$, compared with scores in *Crmp4*+/+ mice. Statistical analysis was performed using the two-way ANOVA test. Data are mean ± S.E.M. (**b**) Photograph of a *Crmp4*+/+ mouse at 4 weeks after SCI demonstrating inability to move with the hindlimbs. (**c,d**) Examples of a *Crmp4*–/– mouse bearing its body weight at 4 weeks after SCI (**c**) and sweeping with the hindlimb at 1 week after SCI (**d**). (Nagai et al., 2015)

Chapter 4. Discussion

Regeneration after CNS trauma is strictly limited by the activations of extrinsic inhibitory pathways related to myelin and scar tissue. Cytoskeleton serves as a intracellular mediator in these pathways to block axonal extension or initiate inflammatory responses for scar formation in CNS[54,57,58,99]. However, there have been no reports that a single intracellular molecule regulates axonal growth and scarring. The current study has two major findings: first, CRMP4 functions both in MAG-induced inhibition of axonal outgrowth and axonal protection in cultured DRG neurons; second, CRMP4 contributes considerably to the inadequate recovery from spinal cord transection *in vivo*.

4.1 CRMP4 in MAG-induced signaling pathways *in vitro*

It has been shown that CRMP4b, the long form CRMP4, is upregualted with MAIs stimulation to interact with RhoA in a PC12 pull-down assay[76]. The same study examined the involvement of CRMP4 in axonal inhibitory signals of Nogo, MAG and OMgp by loss-of-function of CRMP4, but the reduction of CRMP4 expression by the siRNA in cultured neurons was imcomplete[76]. By using *Crmp4*−/− mice in which

complete loss of CRMP4 has been shown[80], I confirmed that CRMP4 deletion in DRG neurons decreases MAG-mediated axonal growth inhibition and growth cone collapse (**Fig. 3.1.1**). In growth cone, the actin-rich peripheral domain and the central domain comprised of microtubules regulate its motility. CRMP4 has been shown to be localized at growth cone and regulates its formation by actin bundling[68,72] and microtubule assembly[71]. It is thus possible that CRMP4 mediates the growth cone collapse after myelin stimulation by controlling cytoskeleton.

CRMP4a, the short form CRMP4, has been shown to regulate microtubule polymerization through its direct binding to tubulin dimers[71]. I tested neuronal sensitivity to VNC, a vinca alkaloid widely used as a chemotherapeutic anticancer agent that leads to mitotic arrest and apoptosis by inhibition of microtubule assembly[82]. In the present study, CRMP4-null DRG neurons exhibited enhanced sensitivity to VNC (**Fig. 3.1.2**). This data supports the possibility that CRMP4a stabilizes microtubule polymerization. However, our preliminary data shows that alteration in distal axonal degeneration (Wallerian degeneration) after axotomy of cultured DRG neurons is not

observed upon CRMP4 deletion, thus the role of CRMP4 in axonal degeneration remains unknown.

Furthermore, I demonstrated that knockout of CRMP4 reduced MAG-induced axonal protection against VNC-mediated acute axonal degeneration (**Fig. 3.1.3**). The dual role of CRMP4 in axonal inhibition and protective signal could be explained by respective involvement of the short and long forms of CRMP4. While CRMP4b interaction with RhoA is increased in MAIs-stimulated cells to mediate the inhibition of axonal elongation, alteration in CRMP4a-RhoA interaction level was not found[76], suggesting that short-form CRMP4 is not involved in the MAI-induced axonal growth inhibition. The other group has reported that MAG binds to another ganglioside receptor and initiates axonal protective responses through a complex of RhoA and unknown molecule[26]. Together with my result, it is conceivable that CRMP4a interacts with RhoA to mediate MAG-induced axonal protection signaling. Although additional studies for further detailed signaling pathways are needed, it was shown that CRMP4 is required for both MAG-induced growth inhibition and protection against toxic insult in

cultured DRG axon. These findings provide new insights into the molecular mechanism of CRMP4-mediated MAG signaling pathways.

4.2 CRMP4 functions after spinal cord injury

The *in vitro* studies showed the dual roles of CRMP4 in MAG-induced signals, but the significance of *Crmp4* deletion after CNS injury *in vivo* has never been examined. The hypothesis that CRMP4 contributes to the limitation of recovery after adult CNS trauma is supported by several major findings from this study on *Crmp4*−/− mice. First, the expression levels of pCRMP4, tCRMP4, and CRMP4b, which are suggested to contribute considerably to limiting axonal growth and to promoting cell death, are significantly increased at the lesion site in spinal cord (**Fig. 3.2.1**). Second, the increased CRMP4 expression in activated microglia/macrophages and reactive astrocytes might contribute to secondary injury, including inflammation and scarring after spinal cord lesion (**Fig. 3.2.2, 3.2.4, 3.2.5**). Third, the deletion of CRMP4 has neuroprotective effects including preservation of microtubule polymerization, cell survival, delayed demyelination, and tissue sparing. This leads to axonal growth and behavioral recovery after SCI (**Fig. 3.2.3, 3.2.6, 3.2.7, 3.2.8, 3.2.9, 3.2.10, and 3.2.11**).

Although cytoskeletal dynamics is commonly involved in several axonal inhibitory responses as well as in the key glial processes during inflammation and scarring[21,54–56], no target molecule has been characterized for the missing link between axon formation and scarring. The current study demonstrates that CRMP4 is a uniquely potent factor for preventing axonal regrowth after SCI through its inhibitory and toxic effects on neurons as well as through its inflammatory effects on reactive astrocytes and microglia/macrophages.

There are several possible explanations for the evident functional recovery at an early stage after SCI in *Crmp4*−/− mice (**Fig. 3.2.11**). First, CRMP4 deletion could diminish the convergent signals from post SCI extracellular inhibitory factors in controlling cytoskeletal dynamics in axons. The involvement of CRMP4 in axonal inhibitory responses *in vitro* has been previously described[75,76,100]. For instance, I have shown that Myelin-associated glycoprotein-induced growth cone collapse and axonal outgrowth inhibition are significantly reduced in cultured DRG neurons from *Crmp4*−/− mice[100]. Moreover, a previous *in vitro* study demonstrated that CRMP4b physically and functionally interacts with RhoA in an MAI-dependent manner, leading to inhibition of

neurite outgrowth[76]. However, the role of CRMP4 in CNS injuries *in vivo* was until now largely unknown. Here, I detected immunoreactivity of CRMP4 co-localized with a neuronal marker in intact and injured spinal cords (**Fig. 3.2.2a,b**), supported by previous studies showing CRMP4 expression in motoneurons in the mutant SOD1 mouse model[89] and after sciatic nerve injury[90]. Moreover, I observed that CRMP4b protein expression was increased in injured axons at 2 h post SCI and that deletion of CRMP4 restored microtubule polymerization at this time point (**Fig. 3.2.1a,g, Fig. 3.2.3**). A previous report showed that RhoA was activated in neurons and glial cells in white matter surrounding the injury site at the same time point after SCI[101]. My findings thus support an inhibitory function of the RhoA-CRMP4b complex in injured spinal cord. Moreover, Sema3A-induced phosphorylation of CRMP4 induces failure of axonal formation and elongation via disruption of CRMP4 binding to microtubules and actin[68,71,72]. It has been reported that Wallerian degeneration is mediated by CRMP phosphorylation[102]. I detected elevation of CRMP4 phosphorylation levels after SCI (**Fig. 3.2.1a,b,f**). Other CRMP family proteins are known to lose their binding affinity to tubulin after Cdk5 and GSK3b phosphorylation. CRMP4 has a shared microtubule

binding domain and phosphorylation sites with other CRMPs[68,69], it is thus possible that phosphorylated forms of CRMP4 also contribute to cytoskeletal degradation during axonal degeneration after SCI. Indeed, *Crmp4*−/− exhibited a suppression of microtubule destabilization and white matter degeneration after spinal cord transection (**Fig. 3.2.3, 3.2.6d, 3.2.7**). Additionally, preliminary experiments in our laboratory showed the reduction of inhibitory response to CSPG in *Crmp4*−/− cultured DRG neurons when compared to a *Crmp4*+/+ control. These results imply that CRMP4 deletion contributed to axonal extension by blocking mediation of MAIs, Sema3A and CSPG-induced growth cone collapse pathways by CRMP4.

Next, CRMP4 deletion had neuroprotective effects on neurons after traumatic lesion, such as decreased apoptosis and neuron loss (**Fig. 3.2.6a-c**), leading to sparing of tissue (**Fig. 3.2.7, 3.2.8**). Calpain is activated in injured spinal cord from a few minutes to several hours after SCI, and is found to induce cell death in motor neurons[103,104]. Activated calpain truncates CRMP4 at the C-terminus and produces a 58-kDa form called tCRMP4, which induces neuronal apoptosis after both *in vitro* neurotoxin treatment and *in vivo* acute traumatic brain injury[78,79]. I detected immediate upregulation

of tCRMP4 post SCI (**Fig. 3.2.1a,e**) and observed a significant decrease in the number of apoptotic cells and loss of neurons after spinal cord transection in *Crmp4*–/– mice (**Fig. 3.2.6a-c**), suggesting that deletion of tCRMP4 suppresses cell death after SCI.

Finally, I observed an early functional recovery in *Crmp4*–/– mice possibly due to reduced acute inflammatory responses and inhibition of scarring (**Fig. 3.2.4, 3.2.5**). Activation of microglia/macrophages, which causes production of proinflammatory cytokines and neurotoxic molecules, is implicated in secondary injury[31]. Reactive astrocytes are the major cellular component of the glial scar, considered as a physical and chemical barrier to CNS regeneration by producing several classes of growth inhibiting molecules[2]. Basically, infiltration of cytotoxic immune cells through permeable BBB after SCI is induced by proinflammatory cytokines from microglia and astrocytes that are activated by cell death in damaged tissue. The initiation of inflammatory processes might be triggered by the other way, such as release of toxic molecules from degenerating axons[105,106]. Therefore, the reduction of the inflammatory response at 1 week post SCI in *Crmp4*–/– (**Fig. 3.2.5a-d**) may have been caused by suppression of microtubule disassembly leading to reduction of axonal degeneration in

a non-cell autonomous manner. Nevertheless, a recent *in vitro* study demonstrated that CRMP4 mediates the migratory and phagocytic capability of activated microglia via CRMP binding to F-actin[107]. I observed a dramatic reduction of non-traumatic inflammation in *Crmp4*−/− spinal cord (**Fig. 3.2.4**) and an upregulation of CRMP4 in activated microglia/macrophages and reactive astrocytes after SCI in control mice (**Fig. 3.2.2c,d**), suggesting a possibility that CRMP4 deletion suppresses inflammation in a cell-autonomous manner *in vivo*. Although further investigation is needed to clarify the molecular mechanisms of the role of CRMP4 in inflammation, my results strongly suggest that a marked reduction of inflammation in this model due to deletion of CRMP4 (**Fig. 3.2.4, 3.2.5a-d**), leading to drastic inhibition of scar formation (**Fig. 3.2.5e-g**), contributes to the early locomotor recovery post SCI (**Fig. 3.2.11**).

I observed that deletion of CRMP4 enhanced immunoreactivities to anti-GAP43 and anti-5-HT antibodies far caudal to the lesion epicenter, suggesting long-distance regrowth, or sprouting of axons including serotonergic raphespinal fibers (**Fig. 3.2.9, 3.2.10a,b,e**). I also identified CST axons using the YFP-H mice[81] where CSTs are clearly visualized as previously described[98]. While YFP-positive main dorsal CSTs

disappeared within and caudal to the lesion site at 4 weeks post SCI in control mice, the genetic deletion of *Crmp4* promoted extensive regrowth or sprouting of a subset of CST axons within and into the distal (caudal) side of the lesion site (**Fig. 3.2.10c,d**). Distally, I observed more apparent YFP signals at the normal location in the main dorsal CST in *Crmp4*–/– mice than in the controls (**Fig. 3.2.10c**), suggesting that these results were due to sprouting of neighboring spared axon terminals rather than regeneration of transected axons. This conclusion seems to be strongly supported by the observed massive decrease of microtubule destabilization (**Fig. 3.2.3**), the decrease in secondary tissue injuries (**Fig. 3.2.5, 3.2.6a, 3.2.6b**), and the sparing of tissue (**Fig. 3.2.6c,d, 3.2.7, 3.2.8**). However, it is particularly challenging to distinguish regeneration from sprouting and to detect inadvertently spared axons, because the CST axons descend through several different tracts[3]. Combinatorial modulations of both intrinsic neuronal mechanisms and extrinsic mechanisms after CNS injuries are required for long-distance axonal regeneration or sprouting and marked functional recovery after SCI[53,108].

It has been reported that the overexpression of intrinsic anti-inflammatory molecules induced locomotor recovery within 1-2 weeks after SCI, which is an early phase of

injury, but the functional regeneration was abolished afterwards[109]. Improved locomotion after injury with elimination of axonal inhibitors was observed from a later phase of SCI. For instance, mice with genetic deletion of NgR showed significant locomotor recovery from 2 weeks after injury[23], and Sema3A inhibitor enhanced locomotor function from 5 weeks after spinal cord transection[39]. My results in this study showed that the significant early locomotor recovery and long-distance axonal regrowth or sprouting caused by CRMP4 deletion were achieved, possibly because both cytoskeletal destabilization in axons and secondary tissue damage were remarkably reduced (**Fig. 4.1**).

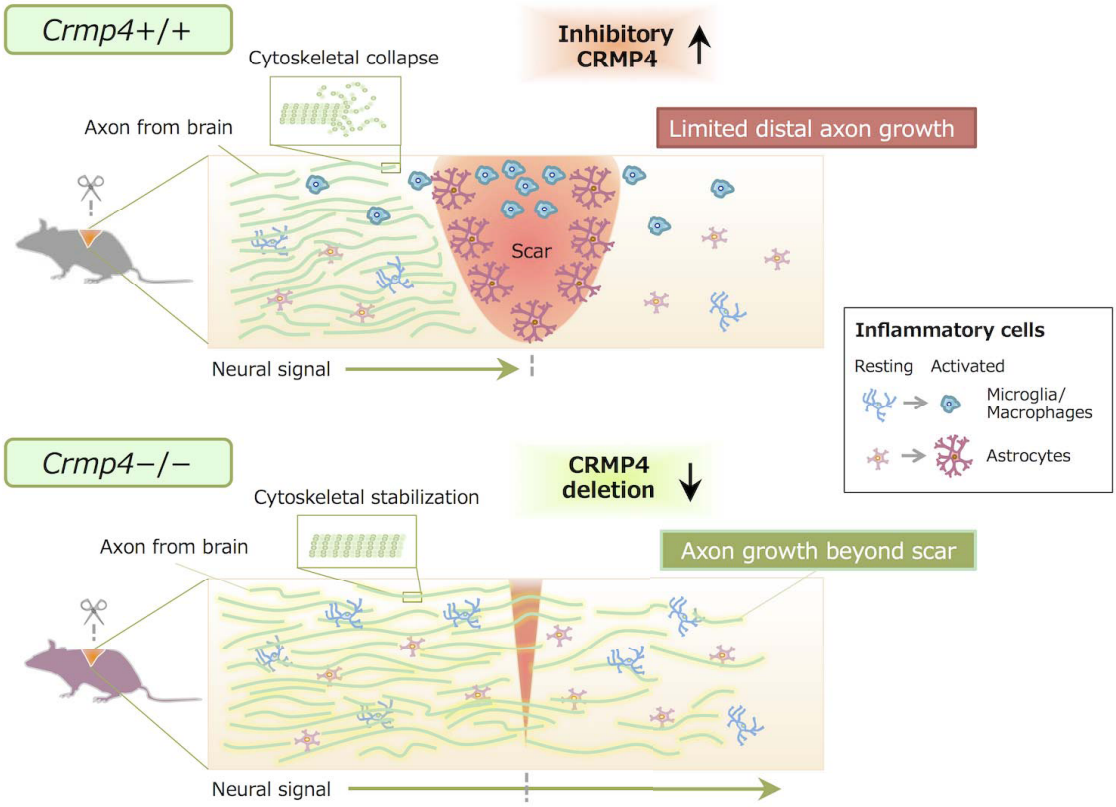

Fig. 4.1 Schematic image of cellular and molecular events in *Crmp4*+/+ and *Crmp4* −/− spinal cords after near-complete transection. In *Crmp4*+/+ mice, cytoskeletal depolymerization occurs in many interrupted axons immediately after SCI, leading to progressive axonal degeneration. Activated inflammatory cells migrate to the injury site to form a scar with connective tissue that expresses and secretes inhibitory molecules to axonal growth. In contrast, CRMP4 deletion stabilizes cytoskeletal polymerization in injured axons and reduces inflammatory activation and subsequent scarring. This promotes axonal growth caudal to the lesion and functional recovery in hindlimb locomotion.

Chapter 5. Future prospects

5.1 Molecular basis regarding CRMP4

In vitro studies in this thesis demonstrated CRMP4 mediates contradictory signaling pathways; inhibition of axon growth and axonal protection from toxic insult (**Fig. 3.1.1-3**). It is possible that different forms of CRMP4 mediate each signal. CRMP4b was dramatically upregulated after *in vivo* injury (**Fig. 3.2.1**). The data that deletion of CRMP4 enhanced regenerative responses after SCI (**Fig. 3.2.9-11**) implicates that inhibitory roles of CRMP4b (possibly, pCRMP4 and tCRMP4 also) might be dominant *in vivo* CNS traumas, however, this is yet to be proven. To examine which form of CRMP4 plays the represented roles, transgenic lines for conditional gene mutation could be effective. Alternatively, for instance, *in vivo* delivery of a peptide of the unique N-terminal domain of CRMP4b (C4RIP– CRMP4b–RhoA inhibitory peptide)[75,76] might be used to assess the role of CRMP4b reduction after CNS injury *in vivo*.

CRMP4 was evident in the injured spinal cords in neurons as well as in reactive astrocytes and activated microglia/macrophages (**Fig. 3.2.2**), raising a hypothesis that CRMP4 regulates inflammatory responses in a cell-autonomous manner *in vivo*.

Additionally, deletion of CRMP4 stabilized cytoskeletal polymerization after spinal transection (**Fig. 3.2.3**), indicating the function of CRMP4 in spinal and cortical neurons. It is not clear which is rather beneficial, the reduction of inflammation and scarring or enhanced axon viability for regenerative responses in *Crmp4*–/– spinal cords. To examine CRMP4 level in each cell types, flow cytometry could be effective. Although the experimental methods using flow cytometry to sort cell types from injured spinal cords are developing, it is still technically difficult to separate neurons and glial cells[110]. Therefore, conditional *Crmp4* depletion in astroglia[111] and/or microglia[112] may be worth trying to clarify that point.

Furthermore, the molecular basis of CRMP4 in inflammatory cells remains largely unknown. Recently a study has shown that CRMP4 binds to F-actin in *in vitro* activated microglial model cells and promotes its migratory property[107]. However, which signaling pathways upregulate CRMP4 expression in reactive astrocytes and in activated microglia/macrophages have never been clearly shown. One of the candidate upstream molecules could be ciliary neurotrophic factor (CNTF). CNTF expression is immediately and predominantly elevated in reactive astrocytes after CNS and PNS

injuries[113] to activate JAK-STAT signaling pathways in glial cells as well as in neurons. JAK-STAT has been suggested to regulate neuronal and inflammatory responses after neural injury[95,114,115]. Increase of CRMP4 mRNA expression was induced by CNTF treatment in cultured neurons[90]. Thus, it is conceivable that CNTF activates JAK to phosphorylate STAT, leading to CRMP4 upregulation after neural injury. To determine that, *in vitro* studies using cultured astrocytes and the murine BV2 microglia cell line could be carried out.

5.2 CRMP4 as a therapeutic target

From a clinical perspective, it is desirable to target molecules with minimal side effects. For instance, the high lethality of *sema3a*−/− mice raises concerns over possible strong side effects of targeting Sema3A[40]. CRMP4 has been shown to be highly expressed in the nervous system[70]. My present results show expression of CRMP4 in neurons, activated microglia/macrophages, and reactive astrocytes, but not in these cells in a resting state. Although detailed behavioral tests need to be conducted, I observed that mice lacking CRMP4 show no gross changes in body growth or fertility. These pieces of evidence suggest that altering CRMP4 expression may have minimal side effects on

other organs when compared to targeting ubiquitous molecules such as RhoA/Rho kinase[20,21] or PTEN/mTOR[116]. Thus, CRMP4 could be a potent candidate target in the development of neuroregenerative medicines. CRMP4b-specific antagonization with C4RIP[75,76] produced by Dr. Founier would be advantageous for use in the complex inhibitory environment prevailing after CNS injury *in vivo*. Additionally, a recently reported antibody that specifically blocks CRMP4 phosphorylation by Dr. Hauberg[117] (patent no. WO 2014139539 A1) might be also effective. However, even though enhanced transportation of a therapeutic antibody inside nervous tissue using a monovalent molecular shuttle was recently reported[118], it is basically hard to pass antibodies through the plasma membrane and target a intracellular molecule, discovery of chemical compound(s) specific to CRMP4 would be thus essential. Alternatively, drugs, enzyme inhibitors and antibodies for upstream molecules of CRMP4 that are under development in clinical trial could have a great potential to control the function of CRMP4 (**Fig. 4.2**).

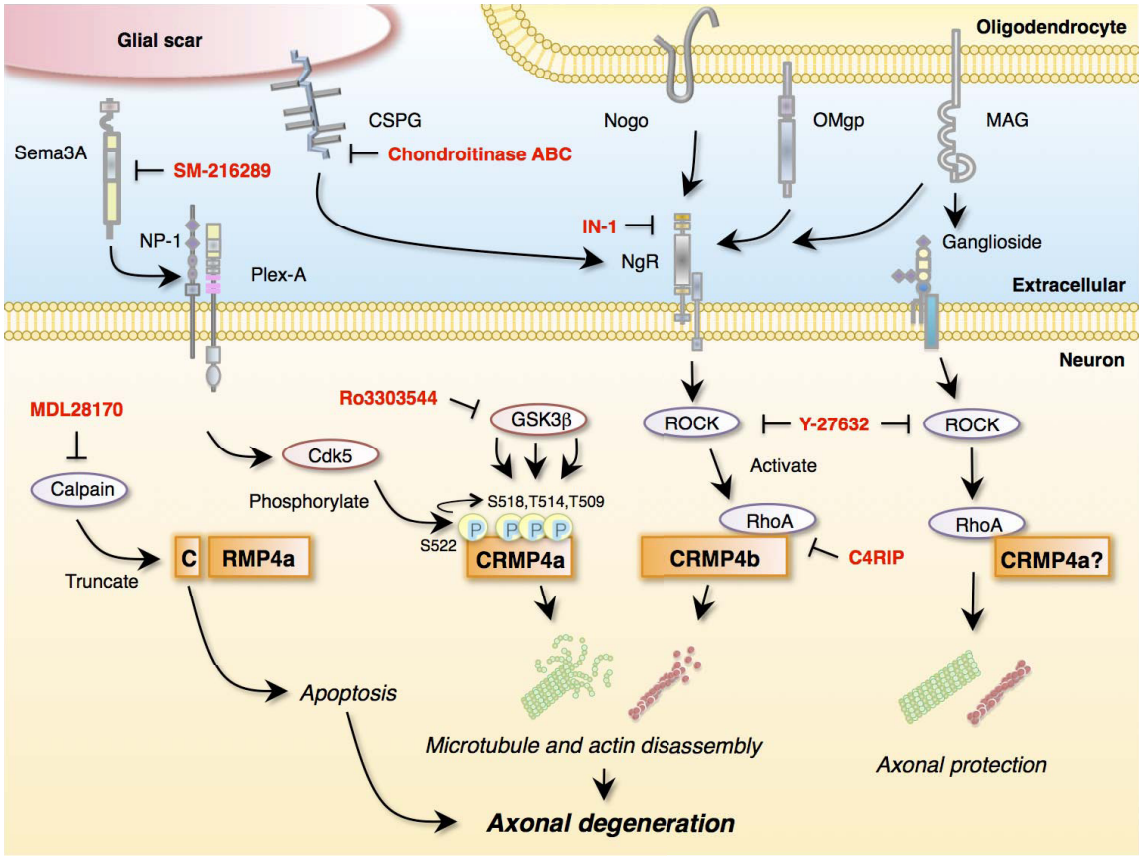

Fig. 4.2 Signaling pathways regarding axonal outgrowth inhibitors and CRMP4.
The drugs, enzyme inhibitors and antibodies for indicated upstream molecules are shown in red characters. SM-216289[39], a selective inhibitor for Sema3A. Chondroitinase ABC[48], an enzyme for CSPG. IN-1[12], an antibody for NgR. MDL28170[119], a chemical inhibitor for calpain. Ro3303544[56], a selective inhibitor for GSK3β. Y-27632[21], a inhibitor for ROCK (Rho kinase). C4RIP[76], an antagonic small peptide for N-terminal domain of CRMP4b, which is implicated to be the interactive region with RhoA.

5.3 Combinatorial treatment with CRMP deletion

Deletion of CRMP4 induced a remarkable functional recovery (BMS score: 5.3 ± 0.3, **Fig. 3.2.11**) after SCI, but this is still not a complete locomotor recovery (BMS score: 9). It points out a possible avenue to combine CRMP4 deletion with other treatments as a therapeutic strategy for further maximal recovery from CNS injury. Permissive cell transplantation to bridge the gap at lesion sites is a prevailing approach. Schwann cell is an abundant source of growth-promoting factors, such as neurotrophins and adhesion molecules[5,10]. Purified Schwann cell grafts into injured murine spinal cords achieved sprouting in motor and sensory nerves[120]. Transplantation of ensheathing glia in olfactory bulb, that has a regenerating system different from the rest of the CNS neurons, promoted restoration of the forepaw motor function[121] and functional regeneration in humans[122]. Whereas the therapeutic potential of stem/progenitor cells for SCI[123,124] from a variety of sources including induced pluripotent stem (iPS) cells[125–127] have been suggested, numerous obstacles present in the surrounding environment, such as secondary tissue damage and the expression of inhibitory molecules associated with scarring, still need to be overcome. Therefore, future directions should focus on the

concurrent regulation of CRMP4 and other treatments/therapeutic modalities such as cell transplantation or neurotrophic factors[128].

In conclusion, the present study demonstrates that deletion of a single protein—CRMP4—resulted in the reduction of axonal outgrowth inhibition in neurons, inflammatory responses of glia, and scarring responses of glia, thereby promoting axonal growth and functional recovery after SCI. Neurological diseases are frequently associated with axonal degeneration and secondary tissue damage by inflammation. My concept that a crucial factor controls both the neuronal and glial responses could be applicable for therapeutic strategies for other diseases in the nervous system. CRMP4 may be a possible therapeutic target for the treatment of human patients with CNS disorders.

References

1. Yiu, G. & He, Z. Glial inhibition of CNS axon regeneration. *Nat Rev Neurosci* **7,** 617–27 (2006).

2. Silver, J. & Miller, J. H. Regeneration beyond the glial scar. *Nat Rev Neurosci* **5,** 146–56 (2004).

3. Tuszynski, M. H. & Steward, O. Concepts and methods for the study of axonal regeneration in the CNS. *Neuron* **74,** 777–91 (2012).

4. Ramón y Cajal, S. Degeneration and regeneration of the nervous system. *New York Oxford UP* (1928).

5. Fawcett, J. W. & Keynes, R. J. Peripheral nerve regeneration. *Annu Rev Neurosci* **13,** 43–60 (1990).

6. Son, Y. J., Trachtenberg, J. T. & Thompson, W. J. Schwann cells induce and guide sprouting and reinnervation of neuromuscular junctions. *Trends Neurosci* **19,** 280–285 (1996).

7. Liuzzi, F. J. & Lasek, R. J. Astrocytes Block Axonal Regeneration in Mammals by Activating the Physiological Stop Pathway.pdf. *Science* **237,** 642–645 (1987).

8. Bray, G. M., Villegas-Pérez, M. P., Vidal-Sanz, M. & Aguayo, a J. The use of peripheral nerve grafts to enhance neuronal survival, promote growth and permit terminal reconnections in the central nervous system of adult rats. *J Exp Biol* **132,** 5–19 (1987).

9. Schwab, M. E. & Thoenen, H. Dissociated neurons regenerate into sciatic but not optic nerve explants in culture irrespective of neurotrophic factors. *J Neurosci* **5,** 2415–2423 (1985).

10. Martini, R. & Schachner, M. Immunoelectron microscopic localization of neural cell adhesion molecules (L1, N-CAM, and myelin-associated glycoprotein) in regenerating adult mouse sciatic nerve. *J Cell Biol* **106,** 1735–1746 (1988).

11. Caroni, P. & Schwab, M. E. Two membrane protein fractions from rat central myelin with inhibitory properties for neurite growth and fibroblast spreading. *J Cell Biol* **106,** 1281–1288 (1988).

12. Caroni, P. & Schwab, M. E. Antibody against myelin-associated inhibitor of neurite growth neutralizes nonpermissive substrate properties of CNS white matter. *Neuron* **1,** 85–96 (1988).

13. Schnell, L. & Schwab, M. E. Axonal regeneration in the rat spinal cord produced by an antibody against myelin-associated neurite growth inhibitors. *Nature* **343,** 269–272 (1990).

14. Filbin, M. T. Myelin-associated inhibitors of axonal regeneration in the adult mammalian CNS. *Nat Rev Neurosci* **4,** 703–13 (2003).

15. McKerracher, L. *et al*. Identification of myelin-associated glycoprotein as a major myelin-derived inhibitor of neurite growth. *Neuron* **13,** 805–811 (1994).

16. Mukhopadhyay, G., Doherty, P., Walsh, F. S., Crocker, P. R. & Filbin, M. T. A novel role for myelin-associated glycoprotein as an inhibitor of axonal regeneration. *Neuron* **13,** 757–767 (1994).

17. Fournier, a E., GrandPre, T. & Strittmatter, S. M. Identification of a receptor mediating Nogo-66 inhibition of axonal regeneration. *Nature* **409,** 341–346 (2001).

18. Wang, K. C. *et al*. Oligodendrocyte-myelin glycoprotein is a Nogo receptor ligand that inhibits neurite outgrowth. *Nature* **417,** 941–944 (2002).

19. Mimura, F. *et al*. Myelin-associated glycoprotein inhibits microtubule assembly by a Rho-kinase-dependent mechanism. *J Biol Chem* **281,** 15970–9 (2006).

20. Dergham, P. *et al*. Rho signaling pathway targeted to promote spinal cord repair. *J Neurosci* **22,** 6570–7 (2002).

21. Fournier, A. E., Takizawa, B. T. & Strittmatter, S. M. Rho kinase inhibition enhances axonal regeneration in the injured CNS. *J Neurosci* **23,** 1416–23 (2003).

22. Lee, J. K. & Zheng, B. Role of myelin-associated inhibitors in axonal repair after spinal cord injury. *Exp Neurol* **235,** 33–42 (2012).

23. Kim, J.-E., Liu, B. P., Park, J. H. & Strittmatter, S. M. Nogo-66 receptor prevents raphespinal and rubrospinal axon regeneration and limits functional recovery from spinal cord injury. *Neuron* **44,** 439–51 (2004).

24. Chivatakarn, O., Kaneko, S., He, Z., Tessier-Lavigne, M. & Giger, R. J. The Nogo-66 receptor NgR1 is required only for the acute growth cone-collapsing but not the chronic growth-inhibitory actions of myelin inhibitors. *J Neurosci* **27,** 7117–24 (2007).

25. Nguyen, T. *et al*. Axonal protective effects of myelin associated glycoprotein. *J Neurosci* **29,** 630–637 (2009).

26. Mehta, N. R., Lopez, P. H. H., Vyas, A. a & Schnaar, R. L. Gangliosides and Nogo receptors independently mediate myelin-associated glycoprotein inhibition of neurite outgrowth in different nerve cells. *J Biol Chem* **282,** 27875–86 (2007).

27. Quarles, R. H. Myelin-associated glycoprotein (MAG): past, present and beyond. *J Neurochem* **100,** 1431–48 (2007).

28. Cao, Z. *et al*. Receptors for myelin inhibitors: Structures and therapeutic opportunities. *Mol Cell Neurosci* **43,** 1–14 (2010).

29. Yin, X. *et al*. Myelin-associated glycoprotein is a myelin signal that modulates the caliber of myelinated axons. *J Neurosci* **18,** 1953–1962 (1998).

30. Pan, B. *et al*. Myelin-associated glycoprotein and complementary axonal ligands, gangliosides, mediate axon stability in the CNS and PNS: Neuropathology and behavioral deficits in single- and double-null mice. *Exp Neurol* **195,** 208–217 (2005).

31. Fitch, M. T., Doller, C., Combs, C. K., Landreth, G. E. & Silver, J. Cellular and molecular mechanisms of glial scarring and progressive cavitation: in vivo and in vitro analysis of inflammation-induced secondary injury after CNS trauma. *J Neurosci* **19,** 8182–98 (1999).

32. Rudge, J. S. & Silver, J. Inhibition of neurite outgrowth on astroglial scars in vitro. *J Neurosci* **10,** 3594–3603 (1990).

33. Preston, E., Webster, J. & Small, D. Characteristics of Sustained Blood-Brain Barrier Opening and Tissue Injury in a Model for Focal Trauma in the Rat. *J Neurotrauma* **18,** 83–92 (2001).

34. Williams, A. *et al*. Semaphorin 3A and 3F: key players in myelin repair in multiple sclerosis? *Brain* **130,** 2554–65 (2007).

35. Gelfand, M. V., Hong, S. & Gu, C. Guidance from above: common cues direct distinct signaling outcomes in vascular and neural patterning. *Trends Cell Biol* **19,** 99–110 (2009).

36. Winter, F. De *et al*. Injury-Induced Class 3 Semaphorin Expression in the Rat Spinal Cord. *Exp Neurol* **175,** 61–75 (2002).

37. Pasterkamp, R. J., Anderson, P. N. & Verhaagen, J. Peripheral nerve injury fails to induce growth of lesioned ascending dorsal column axons into spinal cord scar tissue expressing the axon repellent Semaphorin3A. *Eur J Neurosci* **13,** 457–471 (2001).

38. Pasterkamp, R. J. *et al*. Expression of the gene encoding the chemorepellent semaphorin III is induced in the fibroblast component of neural scar tissue

formed following injuries of adult but not neonatal CNS. *Mol Cell Neurosci* **13,** 143–166 (1999).

39. Kaneko, S. *et al*. A selective Sema3A inhibitor enhances regenerative responses and functional recovery of the injured spinal cord. *Nat Med* **12,** 1380–1389 (2006).

40. Taniguchi, M. *et al*. Disruption of semaphorin III/D gene causes severe abnormality in peripheral nerve projection. *Neuron* **19,** 519–30 (1997).

41. Behar, O., Golden, J. A., Mashimo, H., Schoen, F. J. & Fishman, M. C. Semaphorin III is needed for normal patterning and growth of nerves, bones and heart. *Nature* **383,** 525–528 (1996).

42. Kagoshima, M., Ito, T., Kitamura, H. & Goshima, Y. Diverse gene expression and function of semaphorins in developing lung: positive and negative regulatory roles of semaphorins in lung branching morphogenesis. *Genes to Cells* **6,** (2001).

43. Snow, D. M., Steindler, D. a & Silver, J. Molecular and cellular characterization of the glial roof plate of the spinal cord and optic tectum: a possible role for a proteoglycan in the development of an axon barrier. *Dev Biol* **138,** 359–376 (1990).

44. Gallo, V., Bertolotto, a & Levi, G. The proteoglycan chondroitin sulfate is present in a subpopulation of cultured astrocytes and in their precursors. *Dev Biol* **123,** 282–285 (1987).

45. Johnson-Green, P. C., Dow, K. E. & Riopelle, R. J. Characterization of glycosaminoglycans produced by primary astrocytes in vitro. *Glia* **4,** 314–321 (1991).

46. Jones, L. L., Margolis, R. U. & Tuszynski, M. H. The chondroitin sulfate proteoglycans neurocan, brevican, phosphacan, and versican are differentially regulated following spinal cord injury. *Exp Neurol* **182,** 399–411 (2003).

47. McKeon, R. J., Schreiber, R. C., Rudge, J. S. & Silver, J. Reduction of neurite outgrowth in a model of glial scarring following CNS injury is correlated with the expression of inhibitory molecules on reactive astrocytes. *J Neurosci* **11,** 3398–3411 (1991).

48. Bradbury, E. J. *et al*. Chondroitinase ABC promotes functional recovery after spinal cord injury. *Nature* **416,** 636–40 (2002).

49. Bradbury, E. J. & Carter, L. M. Manipulating the glial scar: Chondroitinase ABC as a therapy for spinal cord injury. *Brain Res Bull* **84,** 306–316 (2011).

50. Ughrin, Y. M., Chen, Z. J. & Levine, J. M. Multiple regions of the NG2 proteoglycan inhibit neurite growth and induce growth cone collapse. *J Neurosci* **23,** 175–186 (2003).

51. Lemons, M. L., Sandy, J. D., Anderson, D. K. & Howland, D. R. Intact aggrecan and chondroitin sulfate-depleted aggrecan core glycoprotein inhibit axon growth in the adult rat spinal cord. *Exp Neurol* **184,** 981–990 (2003).

52. Bracken, M. B. *et al*. A randomized, controlled trial of methylprednisolone or naloxone in the treatment of acute spinal-cord injury. Results of the Second National Acute Spinal Cord Injury Study. *N Engl J Med* **323,** 1645–1650 (1990).

53. Liu, K., Tedeschi, A., Park, K. K. & He, Z. Neuronal Intrinsic Mechanisms of Axon Regeneration. *Annu Rev Neurosci* **34,** 131–152 (2011).

54. Hellal, F. *et al*. Microtubule stabilization reduces scarring and causes axon regeneration after spinal cord injury. *Science* **331,** 928–31 (2011).

55. Westermann, S. & Weber, K. Post-translational modifications regulate microtubule function. *Nat Rev Mol Cell Biol* **4,** 938 (2003).

56. Renault-Mihara, F. *et al*. Beneficial compaction of spinal cord lesion by migrating astrocytes through glycogen synthase kinase-3 inhibition. *EMBO Mol Med* **3,** 682–96 (2011).

57. Witte, H., Neukirchen, D. & Bradke, F. Microtubule stabilization specifies initial neuronal polarization. *J Cell Biol* **180,** 619–32 (2008).

58. Ertürk, A., Hellal, F., Enes, J. & Bradke, F. Disorganized microtubules underlie the formation of retraction bulbs and the failure of axonal regeneration. *J Neurosci* **27,** 9169–80 (2007).

59. Goshima, Y., Nakamura, F., Strittmatter, P. & Strittmatter, S. M. Collapsin-induced growth cone collapse mediated by an intracellular protein related to UNC-33. *Nature* **376,** 509–514 (1995).

60. Minturn, J. E., Fryer, H. J., Geschwind, D. H. & Hockfield, S. TOAD-64, a gene expressed early in neuronal differentiation in the rat, is related to unc-33, a C. elegans gene involved in axon outgrowth. *J Neurosci* **15,** 6757–66 (1995).

61. Byk, T., Dobransky, T., Cifuentes-Diaz, C. & Sobel, a. Identification and molecular characterization of Unc-33-like phosphoprotein (Ulip), a putative mammalian homolog of the axonal guidance-associated unc-33 gene product. *J Neurosci* **16,** 688–701 (1996).

62. Gaetano, C. Identification and Characterization of a Retinoic Acid-regulated Human Homologue of the unc-33-like Phosphoprotein Gene (hUlip) from Neuroblastoma Cells. *J Biol Chem* **272,** 12195–12201 (1997).

63. Inatome, R. *et al*. Identification of CRAM, a novel unc-33 gene family protein that associates with CRMP3 and protein-tyrosine kinase(s) in the developing rat brain. *J Biol Chem* **275,** 27291–302 (2000).

64. Wang, L. H. & Strittmatter, S. M. A family of rat CRMP genes is differentially expressed in the nervous system. *J Neurosci* **16,** 6197–207 (1996).

65. Wang, L. H. & Strittmatter, S. M. Brain CRMP forms heterotetramers similar to liver dihydropyrimidinase. *J Neurochem* **69,** 2261–9 (1997).

66. Deo, R. C. *et al*. Structural bases for CRMP function in plexin-dependent semaphorin3A signaling. *EMBO J* **23,** 9–22 (2004).

67. Charrier, E. *et al*. Collapsin Response Mediator Proteins (CRMPs). *Mol Neurobiol* **28,** 51–63 (2003).

68. Cole, A. R. *et al*. Distinct Priming Kinases Contribute to Differential Regulation of Collapsin Response Mediator Proteins by Glycogen Synthase kinase-3 in vivo. *J Biol Chem* **281,** 16591–16598 (2006).

69. Lin, P.-C., Chan, P. M., Hall, C. & Manser, E. Collapsin response mediator proteins (CRMPs) are a new class of microtubule-associated protein (MAP) that selectively interacts with assembled microtubules via a taxol-sensitive binding interaction. *J Biol Chem* **286,** 41466–78 (2011).

70. Yamashita, N. & Goshima, Y. Collapsin response mediator proteins regulate neuronal development and plasticity by switching their phosphorylation status. *Mol Neurobiol* **45,** 234–46 (2012).

71. Fukata, Y. *et al*. CRMP-2 binds to tubulin heterodimers to promote microtubule assembly. *Nat Cell Biol* **4,** 583–91 (2002).

72. Rosslenbroich, V. *et al*. Collapsin response mediator protein-4 regulates F-actin bundling. *Exp Cell Res* **310,** 434–44 (2005).

73. Quinn, C. C. *et al*. TUC-4b, a novel TUC family variant, regulates neurite outgrowth and associates with vesicles in the growth cone. *J Neurosci* **23,** 2815–23 (2003).

74. Yuasa-Kawada, J. *et al*. Axonal morphogenesis controlled by antagonistic roles of two CRMP subtypes in microtubule organization. *Eur J Neurosci* **17,** 2329–2343 (2003).

75. Alabed, Y. Z., Pool, M., Ong Tone, S., Sutherland, C. & Fournier, A. E. GSK3 beta regulates myelin-dependent axon outgrowth inhibition through CRMP4. *J Neurosci* **30,** 5635–43 (2010).

76. Alabed, Y. Z., Pool, M., Ong Tone, S. & Fournier, A. E. Identification of CRMP4 as a convergent regulator of axon outgrowth inhibition. *J Neurosci* **27,** 1702–11 (2007).

77. Dickendesher, T. L. *et al*. NgR1 and NgR3 are receptors for chondroitin sulfate proteoglycans. *Nat Neurosci* **15,** 703–712 (2012).

78. Zhang, Z. *et al*. Calpain-Mediated Collapsin Response Mediator Protein-1, -2, And -4 Proteolysis after Neurotoxic And Traumatic Brain Injury. *J Neurotrauma* **24,** 460–472 (2007).

79. Liu, W. *et al*. Calpain-truncated CRMP-3 and -4 contribute to potassium deprivation-induced apoptosis of cerebellar granule neurons. *Proteomics* **9,** 3712–28 (2009).

80. Niisato, E. *et al*. CRMP4 suppresses apical dendrite bifurcation of CA1 pyramidal neurons in the mouse hippocampus. *Dev Neurobiol* **72,** 1447–57 (2012).

81. Feng, G. *et al*. Imaging neuronal subsets in transgenic mice expressing multiple spectral variants of GFP. *Neuron* **28,** 41–51 (2000).

82. Wang, M., Wu, Y., Culver, D. G. & Glass, J. D. The gene for slow Wallerian degeneration (Wld(s)) is also protective against vincristine neuropathy. *Neurobiol Dis* **8,** 155–61 (2001).

83. Popovich, P. G. *et al*. The neuropathological and behavioral consequences of intraspinal microglial/macrophage activation. *J Neuropathol Exp Neurol* **61,** 623–33 (2002).

84. Ohshima, T. *et al*. Cdk5 is required for multipolar-to-bipolar transition during radial neuronal migration and proper dendrite development of pyramidal neurons in the cerebral cortex. *Development* **134,** 2273–82 (2007).

85. Park, S. *et al*. Thiazolidinedione class of peroxisome proliferator-activated receptor γ agonists prevents neuronal damage, motor dysfunction, myelin loss, neuropathic pain, and inflammation after spinal cord. *J Pharmacol Exp Ther* **320,** 1002–1012 (2007).

86. Basso, D. M. *et al*. Basso Mouse Scale for Locomotion Detects Differences in Recovery after Spinal Cord Injury in Five Common Mouse Strains. *J Neurotrauma* **23,** 635–659 (2006).

87. Boutros, M. & Ahringer, J. The art and design of genetic screens: RNA interference. *Nat Rev Genet* **9,** 554–566 (2008).

88. Niisato, E. *et al*. Phosphorylation of CRMP2 is involved in proper bifurcation of the apical dendrite of hippocampal CA1 pyramidal neurons. *Dev Neurobiol* **73,** 142–51 (2013).

89. Duplan, L. *et al*. Collapsin response mediator protein 4a (CRMP4a) is upregulated in motoneurons of mutant SOD1 mice and can trigger motoneuron axonal degeneration and cell death. *J Neurosci* **30,** 785–96 (2010).

90. Jang, S. Y. *et al*. Injury-induced CRMP4 expression in adult sensory neurons; a possible target gene for ciliary neurotrophic factor. *Neurosci Lett* **485,** 37–42 (2010).

91. Tumosa, N. & Baker, J. R. Microglia in the nerve fiber layer of the cat retina: detection of postnatal changes by a new monoclonal antibody. *Vis Neurosci* **13,** 671–82 (1996).

92. Hains, B. C. & Waxman, S. G. Activated Microglia Contribute to the Maintenance of Chronic Pain after Spinal Cord Injury. *J Neurosci* **26,** 4308–4317 (2006).

93. Zhang, F. *et al*. Selective activation of microglia in spinal cord but not higher cortical regions following nerve injury in adult mouse. *Mol Pain* **4,** 1–16 (2008).

94. Okada, S. *et al*. Conditional ablation of Stat3 or Socs3 discloses a dual role for reactive astrocytes after spinal cord injury. *Nat Med* **12,** 829–834 (2006).

95. Herrmann, J. E. *et al*. STAT3 is a Critical Regulator of Astrogliosis and Scar Formation after Spinal Cord Injury. *J Neurosci* **28,** 7231–7243 (2008).

96. Liu, X. Z. *et al*. Neuronal and Glial Apoptosis after Traumatic Spinal Cord Injury. *J Neurosci* **17,** 5395–5406 (1997).

97. Hill, R. L. *et al*. Anatomical and Functional Outcomes following a Precise, Graded, Dorsal Laceration Spinal Cord Injury in C57BL/6 Mice. *J Neurotrauma* **15,** 1–15 (2009).

98. Carter, L. M. *et al*. The yellow fluorescent protein (YFP-H) mouse reveals neuroprotection as a novel mechanism underlying chondroitinase ABC-mediated repair after spinal cord injury. *J Neurosci* **28,** 14107–20 (2008).

99. Hsieh, S. H.-K., Ferraro, G. B. & Fournier, A. E. Myelin-associated inhibitors regulate cofilin phosphorylation and neuronal inhibition through LIM kinase and Slingshot phosphatase. *J Neurosci* **26,** 1006–15 (2006).

100. Nagai, J., Goshima, Y. & Ohshima, T. CRMP4 mediates MAG-induced inhibition of axonal outgrowth and protection against Vincristine-induced axonal degeneration. *Neurosci Lett* **519,** 56–61 (2012).

101. Dubreuil, C. I., Winton, M. J. & McKerracher, L. Rho activation patterns after spinal cord injury and the role of activated Rho in apoptosis in the central nervous system. *J Cell Biol* **162,** 233–43 (2003).

102. Wakatsuki, S., Saitoh, F. & Araki, T. ZNRF1 promotes Wallerian degeneration by degrading AKT to induce GSK3B-dependent CRMP2 phosphorylation. *Nat Cell Biol* **13,** 1415–23 (2011).

103. Banik, N. L., Hogan, E. L., Powers, J. M. & Smith, K. P. Proteolytic enzymes in experimental spinal cord injury. *J Neurol Sci* **73,** 245–56 (1986).

104. Springer, J. E., Azbill, R. D., Kennedy, S. E., George, J. & Geddes, J. W. Rapid calpain I activation and cytoskeletal protein degradation following traumatic spinal cord injury: attenuation with riluzole pretreatment. *J Neurochem* **69,** 1592–600 (1997).

105. Mcdonald, J. W., Althomsons, S. P., Hyrc, K. L., Choi, D. & Goldberg, M. P. Oligodendrocytes from forebrain are highly vulnerable to AMPA/kainate receptor-mediated excitotoxicity. *Nat Med* **4,** 291–297 (1998).

106. Beattie, M. S., Farooqui, A. A. & Bresnahan, J. C. Review of Current Evidence for Apoptosis After Spinal Cord Injury. *J Neurotrauma* **17,** 915–925 (2000).

107. Manivannan, J., Tay, S. S. W., Ling, E. & Dheen, S. T. Dihydropyrimidinase-like 3 regulates the inflammatory response of activated microglia. *Neuroscience* **253,** 40–54 (2013).

108. Takeuchi, K. *et al*. Chondroitin sulphate N-acetylgalactosaminyl-transferase-1 inhibits recovery from neural injury. *Nat Commun* **4,** 2740 (2013).

109. Ghasemlou, N. *et al*. Beneficial effects of secretory leukocyte protease inhibitor after spinal cord injury. *Brain* **133,** 126–38 (2010).

110. Beck, K. D. *et al*. Quantitative analysis of cellular inflammation after traumatic spinal cord injury: Evidence for a multiphasic inflammatory response in the acute to chronic environment. *Brain* **133,** 433–447 (2010).

111. Hirrlinger, P. G., Scheller, A., Braun, C., Hirrlinger, J. & Kirchhoff, F. Temporal control of gene recombination in astrocytes by transgenic expression of the tamoxifen-inducible DNA recombinase variant CreERT2. *Glia* **54,** 11–20 (2006).

112. Goldmann, T. *et al*. A new type of microglia gene targeting shows TAK1 to be pivotal in CNS autoimmune inflammation. *Nat Neurosci* **16,** 1618–1626 (2013).

113. Kang, S. S., Keasey, M. P., Cai, J. & Hagg, T. Loss of neuron-astroglial interaction rapidly induces protective CNTF expression after stroke in mice. *J Neurosci* **32,** 9277–87 (2012).

114. Kim, O. S., Park, E. J., Joe, E., Jou, I. & Chem, J. B. JAK-STAT Signaling Mediates Gangliosides-induced Inflammatory Responses in Brain Microglial Cells. *J Biol Chem* **277,** 40594 (2002).

115. Yamauchi, K. *et al*. Activation of JAK/STAT signalling in neurons following spinal cord injury in mice. *J Neurochem* **96,** 1060–70 (2006).

116. Liu, K. *et al*. PTEN deletion enhances the regenerative ability of adult corticospinal neurons. *Nat Neurosci* **13,** 1075–81 (2010).

117. Prashar, P., Swaroop Yadav, P., Samarjeet, F. & Bandyopadhyay, A. Microarray meta-analysis identifies evolutionarily conserved BMP signaling targets in developing long bones. *Dev Biol* **389,** 192–207 (2014).

118. Niewoehner, J. *et al*. Increased Brain Penetration and Potency of a Therapeutic Antibody Using a Monovalent Molecular Shuttle. *Neuron* **81,** 49–60 (2014).

119. Yu, C.-G., Joshi, A. & Geddes, J. W. Intraspinal MDL28170 microinjection improves functional and pathological outcome following spinal cord injury. *J Neurotrauma* **25,** 833–40 (2008).

120. Li, Y. & Raisman, G. Schwann Cells Induce Sprouting Adult Rat Spinal Cord in Motor and Sensory Axons in the Adult Rat Spinal Cord. *J Neurosci* **14,** 4050–4063 (1994).

121. Ramón-Cueto, A., Plant, G. W., Avila, J. & Bunge, M. B. Long-distance axonal regeneration in the transected adult rat spinal cord is promoted by olfactory ensheathing glia transplants. *J Neurosci* **18,** 3803–3815 (1998).

122. Tabakow, P. *et al*. Functional Regeneration of Supraspinal Connections in a Patient With Transected Spinal Cord Following Transplantation of Bulbar

Olfactory Ensheathing Cells With Peripheral Nerve Bridging.pdf. *Cell Transplant* **23,** 1631–1655 (2014).

123. Iwashita, Y., Kawaguchi, S. & Murata, M. Restoration of function by replacement of spinal cord segments in the rat. *Nature* **367,** 167–170 (1994).

124. Lu, P. *et al*. Long-distance growth and connectivity of neural stem cells after severe spinal cord injury. *Cell* **150,** 1264–1273 (2012).

125. Tsuji, O. *et al*. Therapeutic potential of appropriately evaluated safe-induced pluripotent stem cells for spinal cord injury. *Proc Natl Acad Sci U S A* **107,** 12704–12709 (2010).

126. Nori, S. *et al*. Grafted human-induced pluripotent stem-cell-derived neurospheres promote motor functional recovery after spinal cord injury in mice. *Proc Natl Acad Sci U S A* **108,** 16825–30 (2011).

127. Lu, P. *et al*. Long-Distance Axonal Growth from Human Induced Pluripotent Stem Cells after Spinal Cord Injury. *Neuron* **83,** 789–796 (2014).

128. Cai, D., Shen, Y., De Bellard, M., Tang, S. & Filbin, M. T. Prior exposure to neurotrophins blocks inhibition of axonal regeneration by MAG and myelin via a cAMP-dependent mechanism. *Neuron* **22,** 89–101 (1999).

Acknowledgements

First and foremost, I would like to give a deep gratitude to my supervisor Dr. Toshio Ohshima. His continuous support and thoughtful guidance kept me enthusiastic for neuroscience research in which I have been interested since childhood.

I am truly grateful to Dr. Takafumi Inoue for the kind encouragement and willing assistance especially in the seminar every 2 weeks. I also want to thank Dr. Kentaro Semba for his insightfull comments and feedbacks.

Sincere gratitude also goes to all collaborators: Dr. Yoshio Goshima, Dr. Kohtaro Takei, Dr. Naoya Yamashita, Mr. Hiromu Ito. They gave me opportunity to progress this research with valuable discussions.

I deeply appreciate the kind and helpful supports of the members from Ohshima laboratory and Inoue laboratory, especially Dr. Emi Niisato, Mr. Yoshiteru Kitamura and Mr. Kazuki Owada. Without them, this thesis has never been completed.

I also want to thank all the professors of my major as well as people at TWIns for giving me a broad perspective to this beautiful scientific field.

Finally, my heartfelt gratitude goes to my family and fiancée. They gave me persistent support and encouragement to many aspects of my life.

This work was supported by grants from Grant-in-Aid for JSPS Fellows and Global COE for Practical Chemical Wisdom Research Grant for Research Assistant.

Achievements

Original articles

1) **Nagai, J.**, Kitamura, Y., Owada, K., Yamashita, N., Takei, K., Goshima, Y., Ohshima, T. *Crmp4* deletion promotes recovery from spinal cord injury by neuroprotection and limited scar formation. *Sci. Rep*., (2015) 5:8269. * selected as a featured article by natureasia.com

2) **Nagai, J.**, Goshima, Y., Ohshima, T. CRMP4 mediates MAG-induced inhibition of axonal outgrowth and protection against Vincristine-induced axonal degeneration. *Neurosci. Lett.*, (2012) 519: 56-61.

3) Niisato, E., **Nagai, J.**, Yamashita, N., Abe, T., Kiyonari, H., Goshima, Y., Ohshima, T. CRMP4 suppresses apical dendrite bifurcation of CA1 pyramidal neurons in the mouse hippocampus. *Dev. Neurobiol.*, (2012) 72(11): 1447-57.

4) Niisato, E., **Nagai, J.**, Yamashita, N., Nakamura, F., Goshima, Y., Ohshima, T. Phosphorylation of CRMP2 is involved in proper bifurcation of the apical dendrite of hippocampal CA1 pyramicdal neurons. *Dev. Neurobiol.*, (2013) 73(2): 142-51.

Conferences

1) **Jun Nagai**, Yoshiteru Kitamura, Kazuki Owada, Yoshio Goshima, Toshio Ohshima. Genetic modifications of Crmp enhance axonal regrowth after spinal cord injury by reducing cytoskeletal destabilization and inflammatory responses. The 37th Annual Meeting of the Molecular Biology Society of Japan. 2014. Yokohama, Japan. (Poster)

2) **Jun Nagai**, Yoshiteru Kitamura, Kazuki Owada, Yoshio Goshima, Toshio Ohshima. Genetic modifications of Crmp enhance axonal regrowth after spinal cord injury by reducing cytoskeletal destabilization and inflammatory responses. SfN Annual Meeting "Neuroscience 2014". Nov. 2014. Washington D.C., USA. (Poster)

3) **Jun Nagai**. The roles of axon guidance molecules CRMPs in regeneration after CNS injury. Associates of Young Researchers of Physiology Forum. Jul. 26th 2014. Tokyo, Japan. (Oral Presentation)

4) **Jun Nagai**, Yoshiteru Kitamura, Naoya Yamashita, Kohtaro Takei, Yoshio Goshima, Toshio Ohshima. Loss of CRMP4 promotes axonal regrowth and recovery after spinal cord injury The 6th HOPE meeting Mar. 2014. (Poster)

5) **Jun Nagai**, Yoshiteru Kitamura, Naoya Yamashita, Kohtaro Takei, Yoshio Goshima, Toshio Ohshima. The role of CRMP in axonal regrowth after spinal cord injury. SfN Annual Meeting "Neuroscience 2013". Nov. 2013. San Deigo, CA, USA. (Poster)

6) **Jun Nagai**, Yoshiteru Kitamura, Naoya Yamashita, Yoshio Goshima, Toshio Ohshima. The roles of CRMP in axonal sprouting and recovery after spinal cord injury. Neuro2013. P2-2-69. Jun. 2013. Kyoto, Japan. (Poster)

7) **Jun Nagai,** Kodai Sasamoto and Toshio Ohshima. The role of Cdk5 kinase activity in GABAergic interneurons in forebrain. The 6th Neurodevelopmental Symposium. Mar. 14th 2013. Saitama, Japan. (Poster)

8) **J. Nagai**, Y. Kitamura, Y. Goshima, T. Ohshima. The role of Collapsin mediator response protein 4 in axonal regeneration and degeneration. The 35th Annual Meeting of the Molecular Biology Society of Japan. Dec. 2012. Fukuoka, Japan. (Poster)

9) **J. Nagai**, Y. Kitamura, Y. Goshima, T. Ohshima. Role of CRMPs in axonal regeneration after spinal cord injury. The 5th Annual Meeting of Japanese Society for Quantitative Biology.. Nov. 2012. Tokyo, Japan. (Poster)

10) **Jun Nagai**, Andrew Brumm and Stanley Thomas Carmichael. In vitro modeling of neurovascular signaling after stroke. The Cross-disciplinary Scholars in Science and Technology (CSST) Final Presentations. Sep. 2011. Los Angeles, CA, USA. (Poster)

Invited Talks

1) Science Bar INCUBATOR, Regeneration in the nervous system by brake release, Apr. 2015. Shinjuku-ku, Tokyo, Japan.

Campus or Departmental Talks

1) **Jun Nagai**, Yoshiteru Kitamura, Kazuki Owada, Yoshio Goshima and Toshio Ohshima, Genetic modifications of *Crmp* promotes recovery from spinal cord injury, The 16th Joint Symposium between the University of Bonn and Waseda University. Feb. 2015. Tokyo, Japan. (Oral Presentation)

2) **Jun Nagai**, *Crmp4* deletion promotes recovery from spinal cord injury, The 1st TWIns Research Exchange Symposium. Oct. 2014. Tokyo, Japan. (Oral Presentation)

3) **J. Nagai**, Y. Kitamura K. Owada, N. Yamashita, K. Takei, Y. Goshima, T. Ohshima. The role of CRMP in axonal regrowth after spinal cord injury. International

Symposium on Integration of Chemistry and Bioscience. P29. 2013. Tokyo, Japan. (Poster)

4) **Jun Nagai**, Role of CRMPs in axonal regeneration after spinal cord injury, German-Japanese Joint Summer Symposium on Health Span Dynamics Waseda University and University of Bonn, P12. Sep. 2012. Bonn, Germany. (Poster and Oral Presentation)

5) **Jun Nagai**, Role of CRMPs in axonal regeneration after spinal cord injury, The 1st Joint Summer Workshop on International Collaboration Research for Life Innovation between the University of Bonn and Waseda University. Sep. 2012. Karuizawa, Japan. (Poster and Oral Presentation)

Awards and honors

1) The Young Investigator Award, The Physiological Society of Japan, Associates of Young Researchers of Physiology, Jul. 26th 2014.

Grants and Fellowships

1) UCLA CSST Program Fellowship ($9,934), Jul. 5th – Sept. 9th 2011.

2) JASSO Student Exchange Support Program (Scholarship For Short-Term Visit/

Short-Term Stay Program) (¥240,000) for visit to UCLA, Jul. – Sep. 2011.

3) JASSO Student Exchange Support Program (Scholarship For Short-Term Visit/ Short-Term Stay Program) (¥80,000) for visit to Life and Medical Science Institute of Bonn University, Sept. 2011.

4) JSPS Research Fellow DC1, Apr. 2013 – Mar. 2016.

5) Grant-in-Aid for JSPS Fellows (25-5321) (¥1,100,000/year), Apr. 2013 – Mar. 2016.

6) Global COE for Practical Chemical Wisdom Research Grant for Research Assistant (¥400,000), Jan. 2014 – Mar. 2014.